Spring 2017

Technique for normalization of cross-linked peptide ion intensity to elucidate enzymatic conformational changes

Donna Hogan
University of New Hampshire, Durham

TECHNIQUE FOR NORMALIZATION OF CROSS-LINKED PEPTIDE ION INTENSITY TO ELUCIDATE ENZYMATIC CONFORMATIONAL CHANGES

By

DONNA HOGAN

B.S. George Mason University, 2012

B.S. University of Mary Washington, 2005

THESIS

Submitted to the University of New Hampshire

in partial fulfillment of

the requirements for the Degree of

Master of Science

in

Biochemistry

May 2017

This thesis has been examined and approved in partial fulfillment of the requirements for the degree of Master of Science in Biochemistry by:

Thesis Director, Dr. Feixia Chu, Assoc. Professor, MCBS

Dr. Rick Cote, Professor, MCBS

Dr. Estelle Hrabak, Assoc. Professor, MCBS

Dr. Tom Laue, Professor, MCBS

On February 8, 2017

Original approval signatures are on file with the University of New Hampshire Graduate School.

Acknowledgements

I owe many thanks to:

First, my advisor, Dr. Feixia Chu, for allowing me the privilege of working in her lab. She took in a wildcard student and never stopped investing in my success. I grew as a scientist and person under her guidance.

Members of my committee, Dr. Rick Cote, Dr. Estelle Hrabak, and Dr. Tom Laue, for very humanely keeping me in touch with reality. Dr. Laue's protein structure/function course continues to serve as my "intuition" when analyzing data. Dr. Hrabak's course taught me to think critically about my process and the things we take for granted, and Dr. Cote for his invaluable guidance, providing a counter weight to my assumptions, and letting me come through his lab like a tornado.

Xiongzhuo Gao's conversations challenged me every day, but with good humor and grace. Sue Matte helped me more than I can even begin to describe, not just for providing me with the crucial enzymes to conduct experiments (Pαβ and PDE6).

Ben Webb for help with UCSF Modeller; Eric Pettersen and Elaine Meng for help with UCSF Chimera.

Yang Tang, for taking me under his wing much longer than any grad student has a right to expect.

Liz Landis, Lauren Kordonowy, Nancy Fernandes, Dr. Manish Jain, and Dr. Susan Matts, for coffee, moral support, friendship, and reality checks.

And always: Sean, Trobby, Amy, Eileen, Oliver, and our families. For pushing me up the hill and unwavering support even when I was the worst.

Dedicated to My Pack

Table of Contents

List of Acronyms and Abbreviations

Instrumentation and Methods

HPLC	high performance liquid chromatography
LCMS	HPLC coupled to mass spectrometry
CXMS	chemical cross-linking coupled to LCMS
MSn	mass spectra of the n^{th} generation product ion
Cryo-EM	cryo-electron microscopy
NMR	nuclear magnetic resonance spectroscopy
HDX	hydrogen-deuterium exchange – mass spectrometry
SAXS	small-angle X-ray scattering
CD	circular dichroism

Proteins and Enzymes

PTM	post-translational modification
RNAPII	RNA polymerase II
Hsp90	heat shock protein, 90 kilodaltons
HtpG	*E. coli* homolog of Hsp90
SN	staphylococcal nuclease
Δ131Δ	truncation mutant of SN
PDE6	phosphodiesterase 6
Pαβ	alpha and beta subunits of PDE6
Pγ	gamma subunit of PDE6

Reagents and Chemistry

DSS	disuccinimidyl suberate cross-linker
BS3	bis(sulfosuccinimidyl) suberate cross-linker
NHS	N-hydroxysulfosuccinimide
SASA	solvent accessible surface area

List of Figures

Chapter 2

Chapter 3

List of Tables

ABSTRACT

TECHNIQUE FOR NORMALIZATION OF CROSS-LINKED PEPTIDE ION INTENSITY TO ELUCIDATE ENZYMATIC CONFORMATIONAL CHANGES

by

Donna Hogan

University of New Hampshire, May 2017

Cross-linking coupled to Liquid Chromatography/Mass Spectrometry (CXMS) has become an invaluable technique for examining protein-protein interactions and monitoring enzymatic conformational changes. Thus far, comparative quantitation of cross-linked peptides measured by their mass spectrometry (MS) ion intensity is employed to deduce residue cross-linking propensity and spatial proximity. Using two distinct conformations of a structurally well-characterized model protein, we examined the correlation of cross-linked peptide MS signals and distances, but were not able to observe any obvious correlation. Conceivably, several physiochemical factors can affect residue reactivities thus MS signal intensity of the corresponding cross-linked peptides. For NHS ester chemical cross-linkers, the NHS ester functionality often undergo hydrolysis simultaneously to produce dead-end cross-links. Importantly, these dead-end cross-links have proved to be a reliable measurement of the cross-linked lysine residues. Therefore, we propose a novel analytical method by which these dead-end cross-links provide important contextual information about the amino acid side chains involved in cross-linking reactions. Normalization of cross-linked peptide ion intensity against the cognate dead-end cross-links yields a value (proportional cross-link intensity) which can provide a basis for comparison across different biochemical conditions or enzyme interaction states. In this work, we use this method in conjunction with isotopically labeled cross-linking reagents to examine the conformational changes on the part of HtpG (the *E. coli* homolog of

Hsp90) and a truncation mutant of one of its client proteins, Staphylococcal Nuclease. Dramatic conformational changes are observed in the client protein as HtpG transitions through its ATPase cycle. Next, we apply label-free quantitation and the proportional cross-link intensity model to the vertebrate retina enzyme Phosphodiesterase 6 (PDE6). Through pair-wise combinations of the catalytic subunits, cyclic GMP, and the inhibitory subunits, we observe conformational changes in response to allosteric binding of regulatory subunits and molecules.

Chapter 1. Introduction and Background

1.1: A brief look at integrative structural biology and protein interactions

The various functions of proteins and protein complexes are carried out on the platform of their three-dimensional structures. Therefore, detailed protein structural information is critical for mechanistic understanding of biological processes inside the cell. Current biophysical methods for protein structural characterization include X-ray crystallography, Nuclear magnetic resonance (NMR) spectroscopy, small angle x-ray scattering (SAXS), hydrogen/deuterium exchange (HDX), chemical cross-linking and mass spectrometry (CXMS), circular dichroism (CD) spectroscopy, and increasingly, cryo-electron microscopy (cryo EM).

X-ray crystallography offers atomic resolution information, thus considered to be the gold standard in structural biology. This technique requires the generation of well-diffracting protein crystals from large quantity of highly purified proteins in homogeneous biochemical and conformational states, which can be particularly challenging to achieve with large or membrane associated proteins [1]. However, if it can be accomplished, the resolution is generally excellent, with resolution on the order of 1-3 Å. Another caveat of this method resides in potential structural artifacts, especially for conformationally flexible enzymes. Since the crystal environment is very different from the cytosolic environment of the cell, the data might differ significantly from the native conformation. NMR also provides high resolution structural information. However, concentrated protein solution is needed to obtain high quality spectra. In addition, it quickly gets challenging to interpret NMR spectra as the size of the protein increases [2]. Single particle cryo-EM has recently started to generate near-atomic resolution structures of

proteins and protein complexes, with the ability to extract different conformations of the same biomolecules and elucidate their actions inside the cell [3, 4]. However, due to the low signal-to-noise ratio of individual images acquired under low electron doses for high-resolution cryo-EM data, tens to hundreds of thousands of images of single particles need to be averaged. Proper processing of cryo-EM data is lengthy and computationally challenging.

Medium resolution data gained from SAXS, HDX, CXMS, and CD can be used in conjunction with other structural information and contributes to the generation of integrative models [5]. Such hybrid approaches have proven useful in solving the structures of the nuclear pore complex [6, 7], the RNA exosome [8], and yeast chromatin [9]. SAXS is useful for molecules in solution, but may be representative of multiple populations of conformations [10]. HDX is particularly useful for examining the surfaces involved in the interaction of protein complexes, since the exchange of hydrogen for deuterium is much more rapid on those which are not shielded by a ligand or interacting protein [12]. CD relies on the differential absorption of circular polarized light by alpha helices and beta sheets. As such, it provides a complementary method for exploring protein stability and intermolecular interactions [13]. Chemical cross-linking combined with LCMS/MS is becoming more widely used in conjunction with integrative modeling techniques, and is discussed in further detail in the next section. Furthermore, structural information acquired from various methods can be combined to provide mechanistic insights, such as tandem affinity purification and MS to determine subunit stoichiometry [8] and CXMS with X-ray crystallography data to elucidate filament formation and subunit interaction dynamics [14].

1.2: Cross-linking combined with LCMS (CXMS)

Chemical cross-linkers are bi-functional molecules of known length and weight, which covalent link residues in spatial proximity [15]. As such, they act as a "molecular stapler", and serve to predict folds, build topology, and determine interaction surfaces. Because the cross-linker are of known length, identification of which amino acid residues are linked together yields binary distance constraints, which can be combined with homology modeling and other experimental data to refine structural models, elucidate protein interactions, and examine conformational changes within a protein or complex. [16, 17].

Among the most commonly used cross-linkers are NHS esters, such as DSS (disuccinimidylsuberate) and BS3 (bis(sulfosuccinimidyl)suberate). These are reactive towards primary amines, including the N-terminus of proteins and side-chain of lysine residues. Both reagents are 11.4 Å long and can be augmented with deuterium or other functional groups to aid in quantitation and differential comparison. Other cross-linkers may be cleavable (to enable peptide sequencing at the MSn level), or photoactivatable, to capture specific interactions [18-21].

Inherent to the use of cross-linkers is the bioinformatic challenge of finding an efficient way to interrogate a database of potential tryptic peptides to determine the cross-linked peptides which are present, and which are linked together. Search strategies and algorithms score the hits on the basis of MS2 spectra quality, and mass accuracy. The peptide search engine used in this work, Protein Prospector (UCSF) treats each cross-linked peptide moiety as regular peptides with mass modifications [22] and accounts for the asymmetric peptide fragmentation observed following collision induced dissociation, and employs a conservative method for ranking potential identities of cross-linked peptides [23, 24].

Amine reactive cross-linkers such as BS3 and DSS undergo a competing side-reaction: hydrolysis with water in the solution, resulting in only one end of the cross-linker reacting with a peptide side-chain. These are sometimes referred to as dead-end, mono-link, or surface modified peptides. This is estimated to occur much more frequently than a complete cross-link [25, 26], and is usually not included in any downstream analysis. Results from CXMS studies have been largely used as binary data, suggesting presence of spatial proximity of cross-linked residues [27, 28]. Several recent studies use quantitative MS signals of cross-linked peptides to directly infer large-scale domain displacement or rearrangements. However, it remains unclear how accurate the conclusions are without determining physicochemical properties of the of cross-linked residues in different biochemical states.

1.3 Objective

In this study, we hypothesize that quantitative MS information from surface modified peptides can be utilized to deconvolute physicochemical properties of cross-linked residues [29] and distance information of cross-linked residues can be derived after proper normalization. In this sense, it is useful to consider the distance information in terms of restraints rather than constraints. Constraint generally refers to a fixed estimate, while restraint implies the use of an energy function in which deviation is allowed with some penalty [30]. Using two well-characterized conformations of a model protein, heat-shock protein 90 (Hsp90), we have assessed the impact of various physiochemical properties on MS ion intensity of cross-linked peptides. We have further developed a method to deconvolute quantitative CXMS data to derive distance information of cross-linked pairs. We applied this method to the complex of *E. coli* Hsp90 (HtpG) and its model client protein, formed in two different nucleotide-binding states. Our quantitative data illustrate distinct interaction modes at different stages of chaperone-

substrate interaction. Using quantitative CXMS method, we analyzed allosteric regulation of phosphodiesterase 6 (PDE6), the central effector enzyme in vision signaling transduction pathway. Our results suggest structural elements that link spatially distinct regulatory domains and catalytic domains, providing mechanistic understanding on PDE6 allosteric regulation.

Chapter 2. HtpG and Cross-link Ion Intensity Normalization

2.1 Introduction

Protein complexes, dynamic in molecular composition and structural conformation, constitute the structural and functional modules of the cell [33, 34]. Information on the architectural organization of protein complexes and the molecular recognition among their subunits is highly desirable for mechanistic understanding of cellular processes. Increasingly, chemical cross-linking and mass spectrometric analysis (CXMS) is providing important contributions to the structural and functional understanding of proteins and protein complexes [34-38]. This approach enables the identification of residues that are close in three-dimensional space but distant in primary sequence, providing intermediate resolution information to guide *de novo* structure prediction [39], protein interface mapping [40-42] and protein complex model building [43]. The robustness and compatibility of the CXMS approach with multiple biochemical methods have made it especially appealing for challenging systems with multiple biochemical composition and conformation states. In addition, CXMS is highly effective in complementing other structural characterization methods and significantly improves the accuracy of structure prediction [44]. Recent developments in bioinformatics have further enhanced the throughput of CXMS data processing and analysis [23, 29, 45-50], enabling its application to large multi-subunit protein complexes [19, 28, 51-55].

While obtaining qualitative information on the spatial proximity of amino acids from CXMS has become nearly routine, the more challenging quantitative analysis has the potential to locate structural elements that distinguish different conformational states [56]. Strategies utilizing isotope-labeled cross-linkers [57, 58] and label-free quantitation of cross-linked peptides [59] have been utilized to elucidate conformational changes in proteins and protein

complexes. However, the yield of cross-linking products is affected by multiple factors, including the distance of cross-linked pairs, solvent accessibility, pKa value [60-62] and protein surface electrostatic topology [63], which makes it difficult to determine the detailed biophysical nature of conformational changes elucidated by quantitative CXMS analysis.

Amine-reactive cross-linkers are widely used in CXMS studies, due to the favorable distribution of lysine residues on protein surfaces. During cross-linking, these reagents can also undergo hydrolysis reactions and generate singly modified lysine residues (dead-end cross-links) [64]. These dead-end cross-links can be utilized to reliably indicate the reactivity of modified lysine residues [60, 65]. Conceivably, proper normalization of quantitative MS data might allow deconvolution of changes in reactivity and distance. In this study, we test this idea with a CXMS study on a large dynamic molecular chaperone.

Heat shock 90 (Hsp90) proteins constitute a highly conserved and ubiquitously expressed chaperone family [66-68]. Hsp90 chaperones stabilize transient near-native conformations of 'client proteins', both suppressing aggregation [69, 70] and regulating protein activities that are essential to cell signaling and adaptive stress responses [71-73]. Hsp90 functions as a homodimer, with each monomer composed of an N-terminal ATP-binding domain (NTD), a middle domain (MD), and a C-terminal dimerization domain (CTD). The chaperone cycle of Hsp90 is coupled to ATP binding and hydrolysis, with multiple conformational states suitable for its interactions with client and co-chaperone proteins [74-76]. ATP binding elicits extensive conformational changes in Hsp90, switching from a V-shaped 'open' conformation to an NTD-dimerized 'closed' conformation. Meanwhile, repositioning of the NTD and MD constructs a catalytically competent ATP-hydrolysis site on each monomer [68].

Previous studies using a model substrate, a partially folded fragment of staphylococcal nuclease (Δ131Δ), and bacterial Hsp90 (HtpG) have elucidated a conformational 'crosstalk' between the chaperone and its substrate, in which substrate binding drives large scale conformational changes in Hsp90 [77, 78]; while Hsp90 remodels the structure of its client [59]. Results from CXMS data elucidate a client-interacting site on Hsp90, in excellent agreement with those reported from both *in vivo* mutagenesis screens [79] and biochemical studies using other Hsp90 model systems [25, 80]. In this study, we use two distinct conformations of the bacterial Hsp90, HtpG, to explore correlations between the distances of cross-linked pairs with signal intensity in MS data and develop a strategy to deconvolute changes in reactivity and distance. With this new method, we investigate the HtpG/Δ131Δ complex and reveal distinct interaction modes between Δ131Δ and HtpG in different nucleotide-bound states. Our results implicate HtpG structural components subject to conformational regulation in the chaperone cycle.

2.2 Materials and Methods

Protein preparation, complex formation and chemical cross-linking

HtpG and Δ131Δ were purified as described previously [56, 73]. The ATP-state HtpG was formed by incubation with 5mM AMPPNP (Adenylyl-imidodiphosphate) in 25 mM HEPES, 25 mM KCl, 5 mM $MgCl_2$, pH 8.5 at 37 °C for 30 min. Cross-linking experiments were carried out with 50-fold molar excess (for HtpG alone) or 10-fold molar excess (for HtpG/Δ131Δ complex) of BS3-d_0 or BS3-d_4 (Peirce) for 1 hour at room temperature. After quenching, light- or heavy-isotope cross-linker treated samples were combined, separated by SDS-PAGE and in-gel digested [41].

Cross-linked peptide identification and quantitation

After in-gel digestion, cross-linked samples were analyzed by LC-MS/MS as described previously [41]. An UltiMate 3000 Autosampler (Dionex Corp., Sunnyvale, CA) injected a 1 µL aliquot of the extracted peptide solution into a 150 µm x 10 cm reverse-phase capillary column packed with C18 resin (pore size 100 Å) at a flow rate of 450 nL/min. The HPLC eluent was directed to the nanoelectrospray ionization source of an LTQ Orbitrap XL mass spectrometer (Thermo Scientific, Waltham, MA). LC-MS/MS data were acquired in information-dependent mode, cycling between MS scans (m/z 315-1,800) in the Orbitrap and low-energy CID analysis of the three most intense multiply charged precursors in the linear ion trap. Cross-linked peptides were identified using UCSF Protein Prospector, based on a bioinformatic strategy described previously [23]. Averaged MS peak heights from the elution time window of cross-linked peptides and dead-end cross-links were used for comparative quantitation. To minimize isotope overlapping, only the 3° and 4° isotopes of the light and heavy isotope-labeled cross-linked peptides and dead-end cross-links were used. Spectra of cross-linked peptides and dead-end cross-links were manually inspected to verify both identification and quantitation.

Normalization, distribution fitting and distance calculation

The median of the MS signal intensity ratios of cross-linked peptides and dead-end cross-links from each cross-linking experiment was used to normalize protein and cross-linker loading. This approach was validated by a tight distribution of MS signal ratios for cross-linked peptides and dead-end cross-links in open state HtpG samples treated with light- or heavy-isotope cross-linker (Fig. 3A). After loading normalization, the MS signal intensity ratios of two dead-end cross-links were used for reactivity normalization, by dividing the MS signal ratio of cross-

linked peptides by the product of MS signal ratios of the two cognate dead-end cross-links. After reactivity normalization, the MS signal ratio of cross-linked peptides indicates the distance-related cross-linking propensity of lysine residues.

Molecular graphics, analyses, and calculations of solvent accessible surface area and distance between Cα of selected lysine residue side chains were performed with the UCSF Chimera package [95]. The pKa values of cross-linked Lys residues were computed using PROPKA [96].

2.3 Results

Quantitative cross-linking of HtpG in open and closed states

With well-characterized structures in various conformational states, the Hsp90 chaperone is an attractive system to study the relationship between cross-linking propensity and structural properties [68]. Previous studies have identified a conformational equilibrium of HtpG, affected by pH and nucleotide-binding [81-83]. We selected two biochemical conditions for HtpG to predominantly populate either the open *apo* or the closed ATP-bound conformation, using a non-hydrolysable ATP analog, AMPPNP. Upon nucleotide binding, each NTD undergoes extensive rotations about the NTD:MD interface, while two monomers come together, dimerizing the NTDs and activating the two ATP catalytic sites. The NTD rotation can be characterized by four pairs of intra-monomer cross-links, with K45 in proximity with K294 and K298 in the open state (Fig. 1A); whereas K229 in proximity with K294 and K298 in the closed state (Fig. 1B).

Figure 1

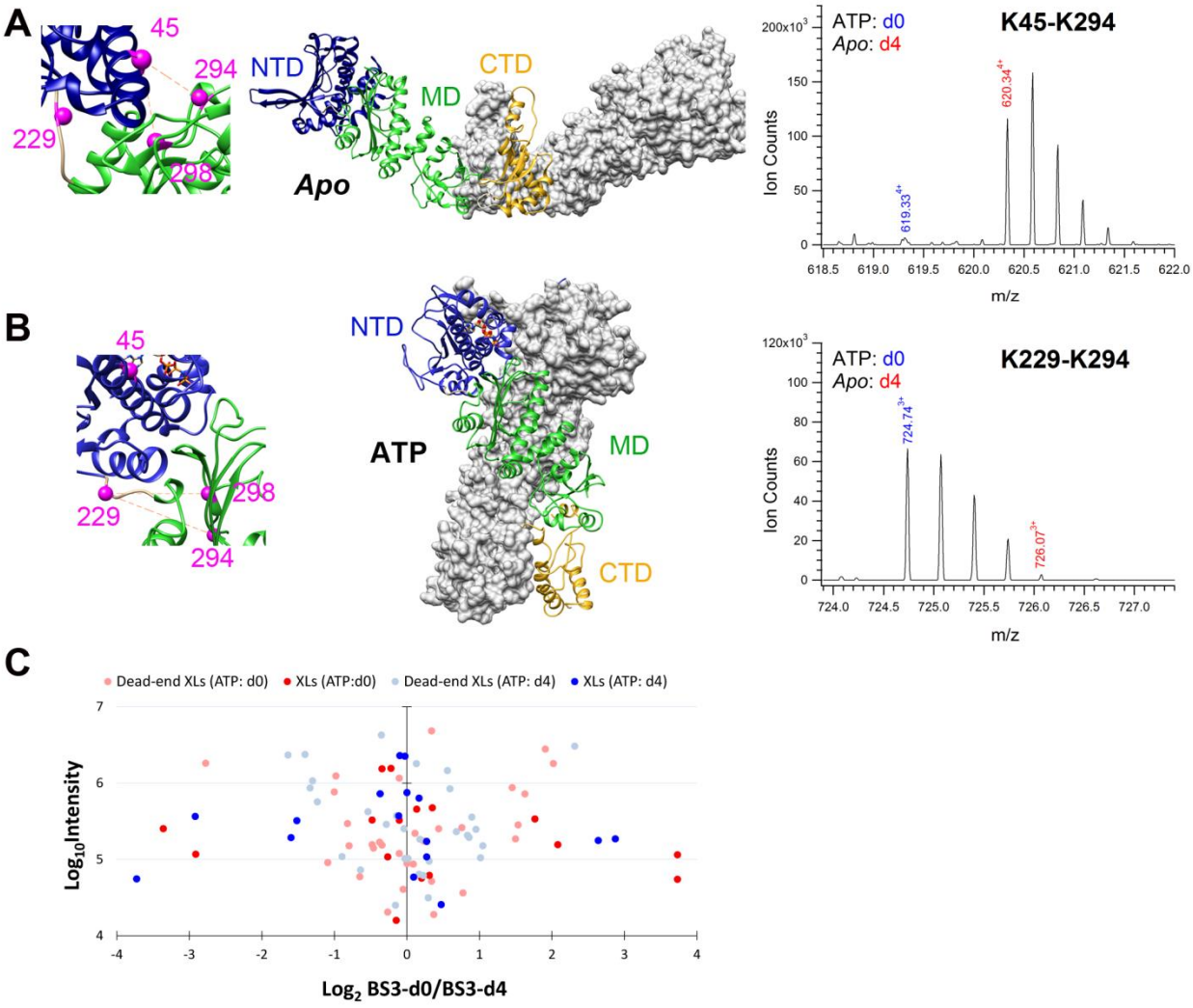

Figure 1. Quantitative cross-linking of HtpG in *apo*- and ATP-state. The NTD/MD interdomain rotation can be characterized by discriminative cross-linked pairs, K45-K294 for *apo*-state (A), K229-K294 for ATP-state (B). (C) L/H ratio and MS ion intensity distribution of cross-linked peptides and dead-end cross-links for forward cross-linking (ATP:d0; *apo*:d4; red dots) and reverse cross-linking (*apo*:d0; ATP:d4; blue dots) experiments.

To probe the structural differences between the open and closed states, HtpG proteins in *apo* open and AMPPNP-bound closed states were cross-linked with heavy-isotope and light-isotope labeled bissulfosuccinimidyl suberate (BS3-d0/light; BS3-d4/heavy), respectively. After the completion of cross-linking reactions, samples were combined and processed for quantitative MS analysis. To assess possible isotope effects on cross-linking reactions, light- or heavy-isotope labeled cross-linkers were swapped for open and closed state. Both forward (open/BS3-d4; closed/BS3-d0) and reverse (open/BS3-d0; closed/BS3-d4) cross-linking experiments were duplicated. Data acquired from four cross-linking experiments were processed separately, and the MS signal ratio of light and heavy isotope was calculated for cross-linked peptides and dead-end cross-links. Each cross-linking experiment generated approximately 30 to 40 MS signal ratios, most of which were for dead-end cross-links. Assuming that the majority of the secondary structures were preserved in the open and closed conformations, we used the median ratio in each cross-linking experiment to normalize for protein and cross-linker loading. Outliers in MS signal ratio were potential candidates, indicating structural elements that are different in open and closed conformations.

As expected, K45-K294 and K45-K298 cross-linked pairs were highly enriched in open state samples; while K229-K294 and K229-K298 cross-linked pairs were highly enriched in closed state samples. The almost exclusive presence of the K45-K294 cross-link in the open state (Fig. 1C; 620.34^{4+}/BS3-d4) and the K229-K294 cross-link in the closed state (Fig. 1C; 724.74^{3+}/BS3-d0) further indicates that under our biochemical conditions HtpG molecules were primarily locked in either open or closed conformation. In addition, we compared the closed/open state ratio of cross-linked peptides and dead-end cross-links between forward and reverse cross-linking experiments (Fig. 3A), and observed consistent ratios between closed and

open states, suggesting that: 1) the effect of heavy/light isotopes in cross-linkers was negligible on quantitative MS data; 2) our dataset was properly normalized for protein and cross-linking reagents loading.

Effects of structural properties on labeling and cross-linking reactions

With comparative quantitation data on two well-defined conformations, we examined the relationship between Cα distances of cross-linked residues and MS signal intensities of the cross-linked peptides. We did not observe any obvious correlation (Fig. 2A). This lack of correlation was not due to large technical variations or the lack of reproducibility, as cross-linking of open state samples with light- or heavy-isotope labeled cross-linkers yielded a tight distribution of MS signal ratios for both cross-linked peptides and dead-end cross-links (Fig. 2B). Physicochemical properties of cross-linked lysine residues can differ in open and closed states, and these may lead to different cross-linking reactivity and yield. Consistent with this notion, the MS signal ratios of some dead-end cross-links from the closed/open dataset were substantially more dispersed (Fig. 3B), in contrast to a tight distribution in open/open dataset (Fig. 2B). Since most dead-end cross-links to a given site exist in significantly higher abundance than inter-peptide cross-links, they can be utilized for relative quantitation of residue reactivity [60-63]. In our dataset, both solvent accessible surface area (SASA) and pKa values (computed by UCSF Chimera [95] and PROPKA [96], respectively) positively correlate with the reactivity of Lys residues when quantitatively measured by dead-end cross-links (Fig. 3A, 3B).

Figure 2

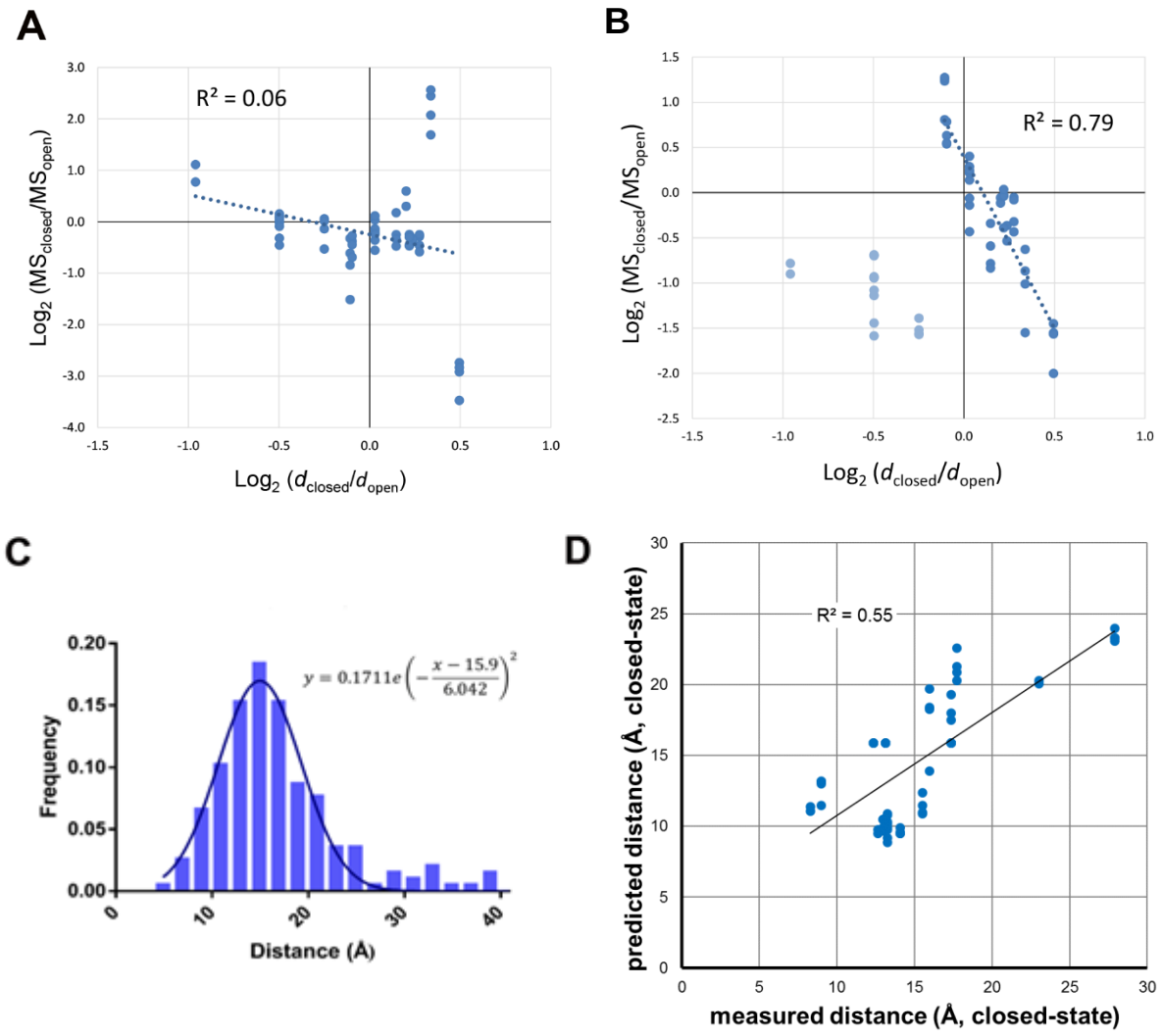

Figure 2. Dissecting effects of residue reactivity and distance in quantitative MS data. Relationship between the distance ratio and MS ion intensity ratio of cross-linked peptides before (A) and after (B) reactivity normalization. (C) The frequency distribution of distances between the Cα of cross-linked residues in RNA polymerase II complex. (D) Relationship between predicted and measured distance values in HtpG ATP-state. Distance values in ATP-state were calculated from *apo*-state distance, distance-frequency distribution and MS L/H ratios.

Figure 3

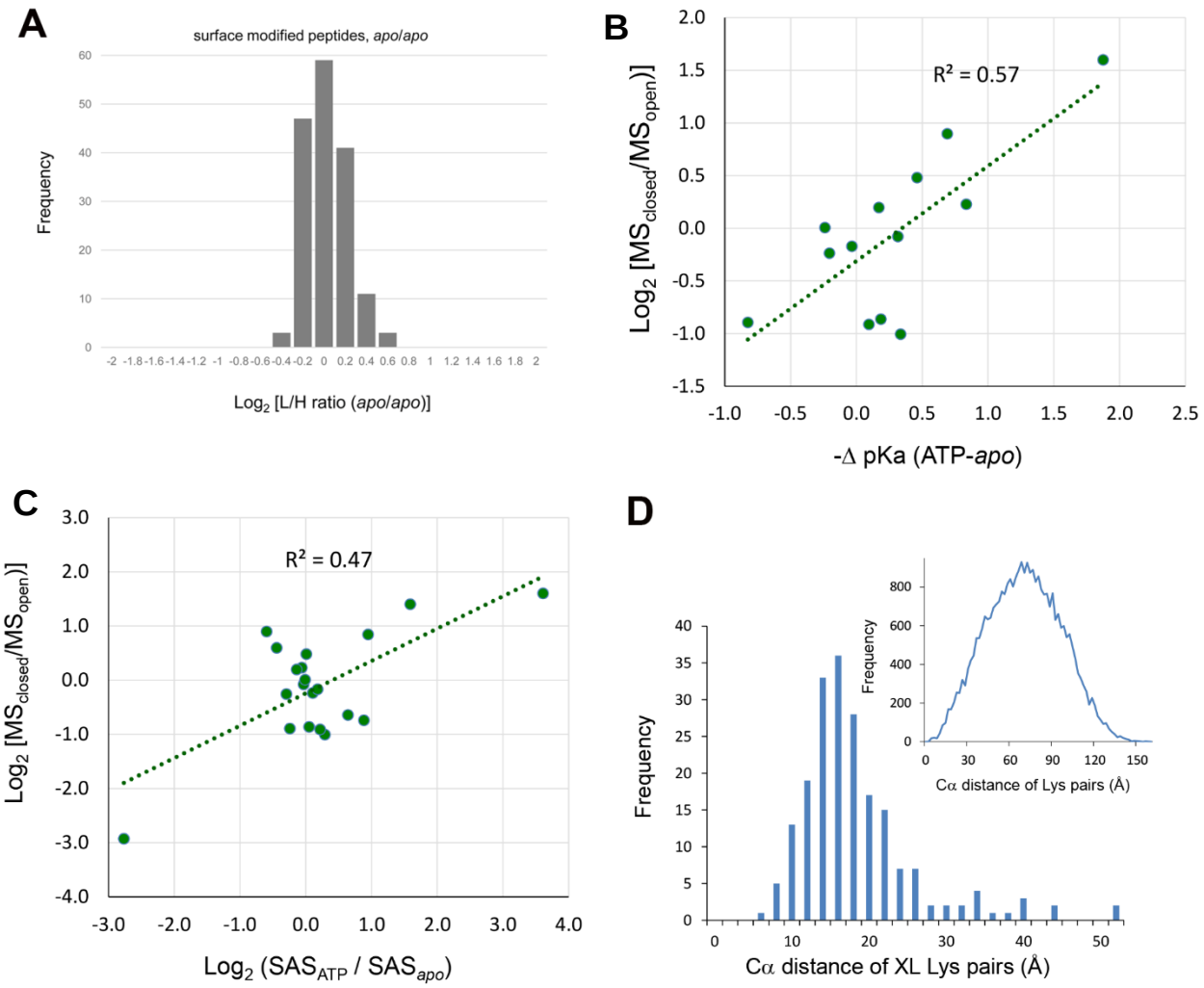

Figure 3. (A) L/H ratio distribution of cross-linked peptides and dead-end cross-links in *apo*-state HtpG treated with light- and heavy-isotope cross-linker. For protein and cross-linker loading, L/H ratios were normalized again the medium of ratios of cross-linked peptides and dead-end cross-links for each cross-linking experiment. Relationship between the reactivity of Lys residues (measured by dead-end cross-links) and pKa value (B), or solvent accessible surface area (SAS) (C). (D) Distance-frequency distribution of all Lys residues in RNA polymerase II complex (PDB, 1wcm).

Assuming a two-step reaction, we used the products of two reactivity ratios of the cross-linked Lys residues to normalize the effect of residue reactivity: $X^*_{ij} = X_{ij}/(D_i*D_j)$ where D_i = MS closed/open signal ratio from the dead-end cross-links. The reactivity ratios of cross-linked Lys residues in closed/open state were measured by the MS signal ratios of corresponding dead-end cross-links in closed/open state. After reactivity normalization, we observed a significantly improved correlation between the log ratios of Cα distance and cross-linked peptide ion intensity (Fig. 2C, blue dots). Most data points populate the upper-left and lower-right quadrants of the plot with a downward trend line, suggesting a negative correlation between the cross-linking probability and distance between cross-linked pairs.

However, a subset of the measurements corresponds to a very different trend line (Fig. 2C, light blue dots). They localize in the lower left quadrant, suggesting a decreased cross-linking propensity in these pairs as residues get closer. These measurements were from three cross-linked pairs of K212/K229, K271/K354 and K502/578, which displayed reduced cross-linking yield while Cα distances decreased in closed form. We inspected various possible structure models, including models built from symmetric yeast Hsp90 [86], asymmetric mitochondria TRAP1 [87], bacteria *apo* HtpG [88] and extended SAX structures [81]. We did not identify steric hindrance or secondary structure changes to rationalize these observations, though we could not eliminate possible effects of local structure dynamics.

A similar effect has been observed in other studies, such as two large-scale cross-linking studies on RNA polymerase II complex using cross-linker BS3 [50, 51]. The frequency distribution of Cα distances of cross-linked Lys residues is bell-shaped (Fig. 2D), distinct from the distance distribution of all available Lys pairs in Pol II complex (PDB 1wcm) (Fig. 2D, inset). Judging from the number of cross-linked pairs, the difference between the two

distributions is not due to sampling saturation. In addition, BS3 (or DSS) cross-linking of other protein complexes also produced bell-shaped distributions with similar boundaries and central maxima [28, 89, 90], suggesting the distance-frequency distribution is independent of protein complexes but intrinsic to the cross-linker.

Our results suggest that the collective behavior of a large population of cross-linked pairs can indicate the distance and cross-linking propensity relationship of individual Lys pairs. Consistent with this idea, all three aforementioned cross-linked pairs have lower cross-linking frequency as their Cα distances decrease. In summary, our results suggest that 1) both residue reactivity and distance contribute to the MS intensity of cross-linked peptides; 2) dead-end cross-links can be used to normalize for reactivity, allowing inference of distance changes; 3) the distance-frequency distribution derived from a large population of cross-linked pairs bears predictive power over an individual cross-link's distance.

Quantitative cross-linking of HtpG/client complex in open and closed states

The chaperone cycle of Hsp90 proteins is coupled to their ATP hydrolysis cycle, where ATP binding, hydrolysis and ADP release lead to conformational changes in Hsp90s and mediate the progression of client folding [68]. Our previous cross-linking studies helped identify an initial substrate binding site in the MD/CTD of HtpG, along with long-range conformational changes on HtpG and Δ131Δ [59, 77, 78]. Having developed a strategy to deconvolute residue reactivity and distance of cross-linked pairs from quantitative cross-linking data, we examined how different nucleotide-binding states affect the interactions between HtpG and its model client, Δ131Δ. We comparatively quantified HtpG/Δ131Δ complexes in open or closed HtpG states using isotope-coded cross-linkers (BS3-d0 or BS3-d4). We observed a reproducible

enrichment of cross-linked HtpG/Δ131Δ complex in the closed state over the open state, which is consistent with a higher affinity between HtpG and Δ131Δ in closed state [77]. As expected, MS quantitation ratios from forward ($closed_{d0}/open_{d4}$) and reverse ($open_{d0}/closed_{d4}$) cross-linking experiments were reciprocal, suggesting minimal isotope effects in cross-linking reactions (Table 1).

After normalization for protein loading and residue reactivity, quantitative data from the cross-linked peptides elucidated two distinct modes of interactions between HtpG and Δ131Δ in the open and closed states (Fig. 4 and Table 1). Though the signal intensity of most intermolecular cross-links skewed towards the closed state, the cross-link between $K103^{HtpG}$ and the N-terminus of Δ131Δ was ~3-fold more abundant in the open state (Fig. 4A). The N-terminus of Δ131Δ cross-linked to only $K103^{HtpG}$ in the open state, in contrast to multiple Lys residues of HtpG in the closed state (Table 1). In addition to residue $K103^{HtpG}$, lysine residues K354 and K560 also formed cross-links to Δ131Δ in the open state HtpG. These residues cluster around a hinge region between the two monomer arms of HtpG in a V-shaped conformation; but are scattered in other open state conformations. A previous study elucidated a shift in HtpG conformation equilibrium towards a V-shaped conformation upon the binding of its substrate [77]. The HtpG cross-linked residues in the open state likely come from this V-shaped conformation, and they delineate a preferred Δ131Δ interaction site near the valley between the two monomers in the open state.

Three additional lysine residues (K229, K294 and K298) formed cross-links to Δ131Δ in the closed state HtpG (Fig. 4B). Lysine residues that show higher Δ131Δ cross-linking

Figure 4

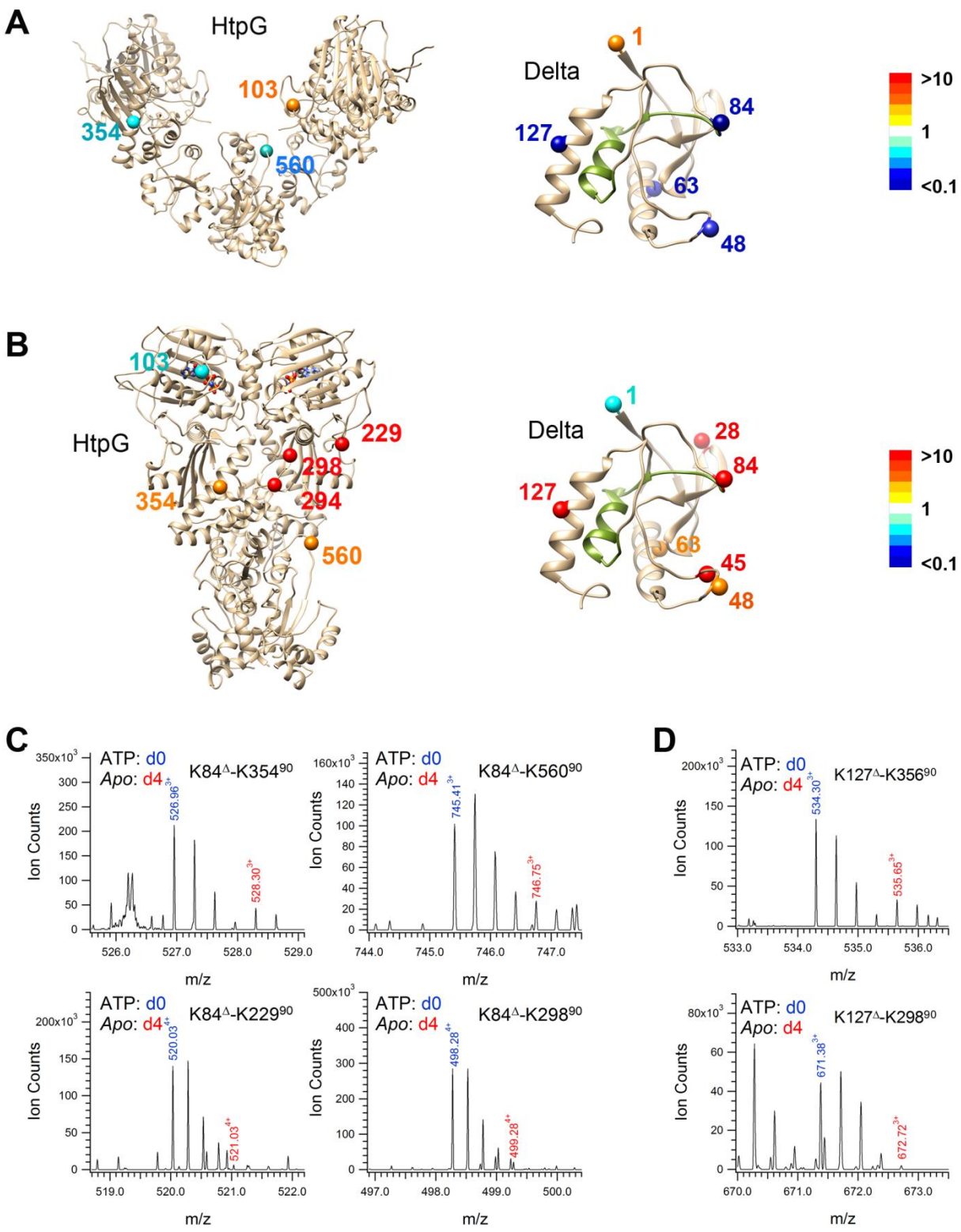
A
HtpG
103
354
560
Delta
1
84
127
63
48
>10
1
<0.1
B
103
HtpG
229
298
354
294
560
Delta
1
28
84
127
63
45
48
>10
1
<0.1
C
ATP: d0
Apo: d4
K84Δ-K354^90
526.96^3+
528.30^3+
Ion Counts
m/z
K84Δ-K560^90
745.41^3+
746.75^3+
K84Δ-K229^90
520.03^4+
521.03^4+
K84Δ-K298^90
498.28^4+
499.28^4+
D
K127Δ-K356^90
534.30^3+
535.65^3+
K127Δ-K298^90
671.38^3+
672.72^3+

Figure 4. Quantitative cross-linking of HtpG/Δ131Δ complex in *apo*- and ATP-state. Residues involved in the intersubunit cross-linking between HtpG and Δ131Δ were mapped back to the structure of *apo*-state (A) or ATP-state (B). Comparative MS quantitation ratios of cross-linked peptides between apo- and ATP-state were color-coded to illustrate nucleotide-dependent interactions between HtpG and Δ131Δ. The native SN structure is shown for Δ131Δ. (C, D) Quantitative MS spectra show preferred interactions between K354 and K560 of HtpG and K84 and K127 of Δ131Δ in ATP-state (blue colored cross-linked peptides) over apo-state (red colored cross-linked peptides). However, the interactions between K229 and K298 of HtpG and K84 and K127 of Δ131Δ are almost exclusive in the ATP-state (blue colored cross-linked peptides).

propensity in the closed state cluster in the MD at an internal cleft of the HtpG dimer. Multiple residues around the MD cleft of yeast Hsp90 produced disappearing peaks in NMR spectra upon the binding of human glucocorticoid receptor [80], corroborating the client binding site on Hsp90 chaperone we detected from the bacterial HtpG/Δ131Δ system. In addition, the NTD rotation during the transition from HtpG open to closed state repositions some residues at the NTD/MD interface, such as K229, K294 and K298, towards the internal cleft of HtpG M-domain. As expected, these residues formed cross-links to Δ131Δ only in the closed state.

Several Δ131Δ residues were involved in cross-linking with HtpG (Fig. 3). Though Δ131Δ is largely unstructured in solution, a region (residue 85-110) has significant structure [90] and interacts with HtpG [93] (Fig. 4A, 4B, colored in olive green). In the native staphylococcal nuclease (SN) structure, this region is flanked by residues that were cross-linked to HtpG. Two Δ131Δ residues near the structured region, K84 and K127, were cross-linked to HtpG K354 and K560 in both the open and closed states (Fig. 4C, 4D). However, they only formed cross-links with HtpG K229, K294 and K298 in the closed state (bottom panel in Fig. 3C, 3D), when these residues were brought to the interacting surface upon NTD rotation. These results validate both the conformational specificity of HtpG under our biochemical conditions and the specificity of cross-linking reactions. Unlike protein complexes held by static interactions, $K84^{\Delta 131\Delta}$ and $K127^{\Delta 131\Delta}$ were crosslinked to several HtpG residues of different regions. Similarly, several HtpG residues were cross-linked to Δ131Δ residues from different regions of the SN native structure. Our results suggest multiple binding orientations between HtpG and Δ131Δ conformers or substantial structural freedom in Δ131Δ conformers.

In addition to interprotein cross-links, multiple intraprotein cross-links were detected among Δ131Δ residues (Table 2). Most pairs had higher or almost unchanged cross-linking

Table 1

Intermolecular cross-links in HtpG/Delta Bands

m/z	z	protein1	A.A. 1	protein2	A.A. 2	**ATP /*Apo***	***Apo*/ATP**
842.4507	3	Delta	A1	HtpG	K103	0.35	3.41
691.068	3	Delta	A1	HtpG	K229	high	low
662.0565	3	Delta	A1	HtpG	K298	high	low
524.9811	3	Delta	A1	HtpG	K354	high	low
743.44	3	Delta	A1	HtpG	K560	high	low
553.5485	4	Delta	K28	HtpG	K354	high	low
707.9094	4	Delta	K45	HtpG	K229	high	low
583.3398	4	Delta	K45	HtpG	K354	high	low
450.2734	3	Delta	K48	HtpG	K354	10.70	0.11
510.2813	4	Delta	K63	HtpG	K354	7.60	0.12
520.0342	4	Delta	K84	HtpG	K229	high	low
498.278	4	Delta	K84	HtpG	K298	high	low
526.9545	3	Delta	K84	HtpG	K354	6.13	0.19
745.4096	3	Delta	K84	HtpG	K560	7.89	0.14
578.3155	3	Delta	K127	HtpG	K294	high	low
671.3806	3	Delta	K127	HtpG	K298	high	low
534.3035	3	Delta	K127	HtpG	K354	3.80	0.33

Table 1. HtpG/Δ131Δ intersubunit cross-linked peptides and their L/H ratios after reactivity normalization.

Table 2

Delta intramolecular cross-links in HtpG/Delta Bands

m/z	z	protein1	A.A. 1	protein2	A.A. 2	**ATP /*Apo***	***Apo*/ATP**
753.4025	3	Delta	A1	Delta	K28	1.46	0.63
591.0969	4	Delta	A1	Delta	K45	1.17	0.91
621.3413	4	Delta	A1	Delta	K53	1.88	0.50
690.3782	3	Delta	A1	Delta	K63	1.98	0.58
707.3875	4	Delta	K45	Delta	K63	1.34	0.75
616.5925	4	Delta	K45	Delta	K70ox	1.46	0.71
592.5789	4	Delta	K45	Delta	K84	1.44	0.72
533.2848	4	Delta	K48	Delta	K53	1.03	1.17
383.9636	4	Delta	K49	Delta	K64ox	1.64	0.56
359.9494	4	Delta	K49	Delta	K84	2.04	0.61
539.5334	4	Delta	K63	Delta	K70	1.52	0.83
743.6447	4	Delta	K64ox	Delta	K97ox	1.58	0.62
546.6215	3	Delta	K84	Delta	K127	0.67	1.73
717.6254	4	Delta	K116	Delta	K127	0.84	1.15

Table 2. Δ131Δ intrasubunit cross-linked peptides in cross-linked HtpG/Δ131Δ complex and their L/H ratios after reactivity normalization.

propensity when in complex with the closed state HtpG, except one pair flanking the Δ131Δ region that interacts with HtpG (K84-K127). In our previous study, the K84-K127 pair displayed the most significant decrease in the closed state, HtpG/Δ131Δ complex when compared to free Δ131Δ [59]. Our current study indicates lower cross-linking propensity in the closed state than open state HtpG/Δ131Δ complex. Together, these results suggest a continuous structure remodeling on substrate Δ131Δ, as chaperone HtpG progresses along its conformational cycle from open to closed state. A possible reason for a wide-spread increase of Δ131Δ intraprotein cross-links in the closed, ATP-state HtpG/Δ131Δ sample might be due to a higher degree of folding in Δ131Δ to favor the formation of a few specific cross-links.

2.4 Discussion

Quantitative cross-linking to deconvolute residue reactivity and distance

The structure of proteins and protein complexes is highly contextual, sensitive towards cellular localization, posttranslational modifications, ligand-binding and oligomerization state. Many proteins have been observed to populate multiple structural conformations [92-94], and subtle changes in primary structure can completely alter the fold and function of a protein [41]. Therefore, biochemical measurements to elucidate conformational changes, in conjunction with a wealth of high-resolution protein structures, can reveal underlying mechanisms of complex cellular processes. The sensitive and robust CXMS approach to elucidate spatial proximity of amino acids offers valuable structural insights, especially on challenging systems that are refractory towards traditional methods. The incorporation of isotope-coded cross-linkers in CXMS can differentially label proteins and protein complexes of different conformational states and implicate conformational changes. However, multiple physiochemical factors can lead to

changes in cross-linking yield. Therefore, quantitative MS data of cross-linked products alone provides only low resolution insights into the nature of conformational changes.

In this study, we examined how various physiochemical factors affect quantitative MS data, and developed a method to deconvolute reactivity and distance of cross-linked residues using quantitative MS data. Using two distinct conformations of HtpG, we demonstrated substantially improved correlation between distance and quantitative MS data of cross-linked pairs after reactivity normalization. Without reactivity normalization, we would not have been able to detect changes in distance-caused cross-linking propensity between K212/K229 and K271/K354 pairs, and would have assigned three other unique cross-linked pairs incorrectly. In addition, for HtpG/Δ131Δ complexes in open and closed states, we would not have been able to identify substantial changes in cross-linking propensity in $K84^{\Delta131\Delta}$/ $K354^{HtpG}$, $K84^{\Delta131\Delta}$/$K560^{HtpG}$, and $K84^{\Delta131\Delta}$/$K127^{\Delta131\Delta}$ pairs, which are likely caused by changes in distance.

Dead-end cross-links are utilized to quantify the reactivity of individual Lys residues, assuming they are the dominant cross-linking products due to the significantly higher concentration of water molecules than that of the pairing Lys residue. However, when reactivity of the side-chain is much higher than water and produce more cross-linking products, dead-end cross-links become less representative for the reactivity of individual residues, leading to less reliable normalization and larger errors.

Nucleotide-dependent, chaperone-substrate interactions in Hsp90 chaperone cycle

Using our reactivity normalization strategy, our quantitative cross-linking analysis of HtpG/Δ131Δ complex in open and closed states revealed different chaperone-substrate interactions, and key structural elements to couple the chaperone and ATP hydrolysis cycle of

Hsp90 molecular chaperones. While residues from the MD/CTD of HtpG were predominantly cross-linked to the more structured region of Δ131Δ, K103 from the NTD of HtpG formed cross-link with the N-terminus of Δ131Δ. Our result is consistent with the notion that HtpG NTD binds to short, unstructured peptides while the MD/CTD binds to more structured substrates [68, 69].

In open state, three HtpG residues (K103, K354 and K560) were cross-linked to Δ131Δ. Lysine residues $K354^{HtpG}$ and $K560^{HtpG}$ formed cross-links with multiple Δ131Δ residues. The resulting cross-linked peptides had higher abundance than the $K103^{HtpG}$/N-$terminus^{\Delta 131\Delta}$ cross-link, suggesting that HtpG MD/CTD constitutes the primary interaction site with Δ131Δ. This is in excellent agreement with previous *in vitro* and *in vivo* studies on HtpG [78, 79]. The secondary interaction site ($K103^{HtpG}$) localizes to the 'lid region' of the nucleotide-binding site in HtpG NTD. It is quite specific in the open state, producing one cross-link with fairly high abundance. A previous study suggests a cross-monomer contact with HtpG NTD can facilitate the unfavorable NTD rotation for the activation of HtpG ATPase activity [78]. Consistent with this idea, a molecular dynamics simulation identifies functional motifs around $K103^{HtpG}$ and $K354^{HtpG}$ that regulate allosteric signaling and interdomain motions of the open, *apo* state HtpG [91]. Interestingly, the activating cochaperone Aha1 binds to a similar region on yeast Hsp90 to accelerate formation of the closed conformation [92]. Therefore, our results suggest that preferred substrate binding near the allosteric elements of HtpG during initial binding might elicit concerted rotations at the NTD/MD and MD/CTD inter-domain surfaces and facilitate the progression of the ATPase cycle in HtpG. This direct coupling of substrate binding with conformational changes in HtpG along the progression of the chaperone cycle provides a feasible functional strategy with reduced dependence on cochaperones.

Chapter 3. PDE6 and Proportional Cross-link Ion Intensity

3.1 Introduction

Phosphodiesterase 6 (PDE6) catalyzes the penultimate reaction in the visual signal transduction cascade in vertebrate photoreceptor cells [97]. This membrane bound enzyme is composed of two catalytic subunits (Pα and Pβ), flanked by two identical inhibitory subunits (Pγ) [98]. Two post-translational modifications on PDE6, isoprenylation on Pα and Pβ, associate the holoenzyme with the membrane of the outer segment of rod photoreceptor cells [99]. The signaling cascade begins when a photon converts 11-cis retinal to all-trans retinal within rhodopsin, which causes a conformational change in rhodopsin such that the alpha subunit of transducin ($G_t\alpha$) dissociates from rhodopsin and displaces the Pγ subunit from the PDE6 holoenzyme (Pαβγγ), thereby relieving inhibition of the catalytic subunit. Pαβ then rapidly hydrolyzes cGMP, which quickly reduces the local concentration of cGMP such that the cGMP-gated ion channels in the membrane close, causing hyperpolarization and the activation of secondary visual neurons. [97-108]

In addition to being inhibited by the Pγ subunits, Pα and Pβ are also allosterically regulated by the binding of cGMP to the non-catalytic binding sites in the GAF domain [102]. The binding of noncatalytic cGMP and Pγ subunit is synergistic [99, 103, 100]. The two catalytic subunits have similar but non-identical amino acid sequence, and the Pγ subunits adopt an extended conformation when associated with Pα and Pβ, physically block the catalytic pocket, and make contact along the length of the GAF domain, as previously elucidated by biochemical and CXMS experiments [41, 101].

Owing to the difficulties in heterologous expression of the holoenzyme and the relatively low quantities that can be purified from tissue, there are many challenges preventing the collection of X-ray crystallography data for this enzyme. Previous studies defined the dimerization interface of the catalytic subunits and the interface between the Pγ and Pαβ subunits, and generated integrative models based on CXMS-derived distance restraints [41]. Chimeras of PDE5/6 revealed an interface between the H and M loops of the catalytic domain that enables binding of Pγ [107]. Binding of Pγ1-60 (a truncated mutant) to the GAF domain does not increase hydrolysis of cGMP in the catalytic domain, but it does increase the binding affinity of both Pγ63-87 and vardenafil to the catalytic domain [103]. In conjunction with drug binding assays, this establishes the cooperative nature of inhibitory ligand binding to the GAF and catalytic domains of Pαβ [103]. This implies allosteric communication between the GAF and catalytic domains. Additionally, cGMP, the first deactivation step, has been shown to initiate a slow conformational change which is accelerated by subsequent binding of Pγ [100]. This work illustrates the structural consequences within the catalytic domain upon binding of cGMP and Pγ using quantitative CXMS. Briefly, we identified several additional structural loops in the catalytic domain which undergo changes depending on the specific ligands bound to Pαβ. These indicate the unique contributions of cGMP and Pγ in the regulation of Pαβ.

3.2 Materials and Methods

Materials – Bovine retinas were purchased from W.L. Lawson, Inc. Trypsin was purchased from Promega. DSS was purchased from Pierce.

Enzyme purification – Bovine rod PDE6 was purified from bovine retinas as described [105]. Pαβ catalytic dimers lacking Pγ were prepared by limited trypsin proteolysis and re-purified by gel filtration chromatography prior to use.

Biochemical and cross-linking conditions – Chemical cross-linking was carried out using 200 molar excess of the cross-linking reagent DSS relative to Pαβ in four different allosteric states: Pαβ alone, Pαβ with cGMP, Pαβ with Pγ, Pαβ with cGMP and Pγ, and PDE6 holoenzyme. The phosphodiesterase inhibitor vardenafil was included whenever cGMP was added to block catalytic activity. Pαβ or PDE6 was present at 2.8 pmol (approximately 0.5 µg in volumes ranging from 10 µL to 20 µL), and incubated with 100 µM vardenafil, and 10 mM EDTA for 40 min at RT where indicated. Reactions with 5 pmol Pγ and 1 mM cGMP were incubated for 10 min. Cross-linking took place for 1 hour at RT, and was quenched with 0.8 M NH_4OH for 15 min. All reactions took place in cross-linking buffer (20 mM HEPES, 20 mM KCl, 5 mM $MgCl_2$ pH 8) and the volume was concentrated from 80 µL to ~30 µL before separation by 4-15% gradient SDS-PAGE.

LCMS sample preparation and analysis – Cross-linked samples were separated by SDS-PAGE followed by in-gel digestion and LCMS/MS analysis as described in Chapter 2.

Data Analysis – Extracted peptides were identified by Protein Prospector per the parameters indicated in Chapter 2. Cross-linked peptide and dead-end cross-link ion intensity was recorded by extracted ion chromatogram using an in-house developed Python script for calculating peak heights and percent cross-link intensity using the formula

$$\%Int = \frac{\sum_Z Crosslink}{\sum_Z Site\ 1 + \ \sum_Z Site\ 2}$$

where site 1 and site 2 are the sum of cross-link intensity across charge states ± 2 of the cognate dead-end peptides.

3.3 Results

Though quantitative CXMS analysis using isotope-coded cross-linkers can provide valuable information on the nature of conformational changes, most commercially available isotope-labeled cross-linkers are supplied in two heavy/light forms, allowing only pair-wise comparison. In addition, using the product of dead-end cross-links can potential magnify the error for residue reactivity normalization (discussed in details in Chapter 2). An alternative approach is to use label-free quantitation, which allows direct comparison of multiple conformations and higher throughput of analysis. Since other physicochemical factors, in addition to the distance of cross-linked residue, affect MS ion intensity of cross-linked peptides, it is important to normalize quantitative MS data with the contribution of residue reactivity. Conceivably, the percentage of molecules that undergo productive cross-linking reactions can be a parameter, independent of residue reactivity and mainly determined by residue distances and local secondary structures. In addition, the competing hydrolysis reaction is a dominant side reaction, producing significantly higher abundance dead-end cross-links than cross-linked peptides for most available cross-linked residues. Therefore, percent cross-link intensity is calculated by dividing the peak height of the cross-linked peptide by the sum of the two cognate dead-end peptides. Larger values indicate an increased cross-linking propensity, and differing values are indicative of more dramatic conformational changes because a larger proportion of the ion intensity is due to the cross-linked peptides rather than either of the dead-end peptides. To probe inter-domain allosteric interactions within Pαβ, we performed cross-linking experiments in four different biochemical conditions as described in Figure 1A. A fifth condition, native

Figure 1

A

i. Pαβ
ii. Pαβ + cGMP
iii. Pαβ + Pγ
iv. Pαβ + cGMP + Pγ
v. PDE6 holoenzyme

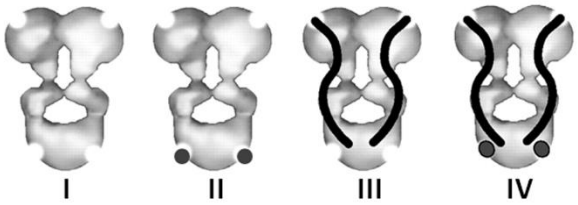

Fig. 1A Pαβ is depicted alone (condition i), with allosteric cGMP bound (condition ii), with Pγ (condition iii), and with both cGMP and Pγ (condition iv)

B

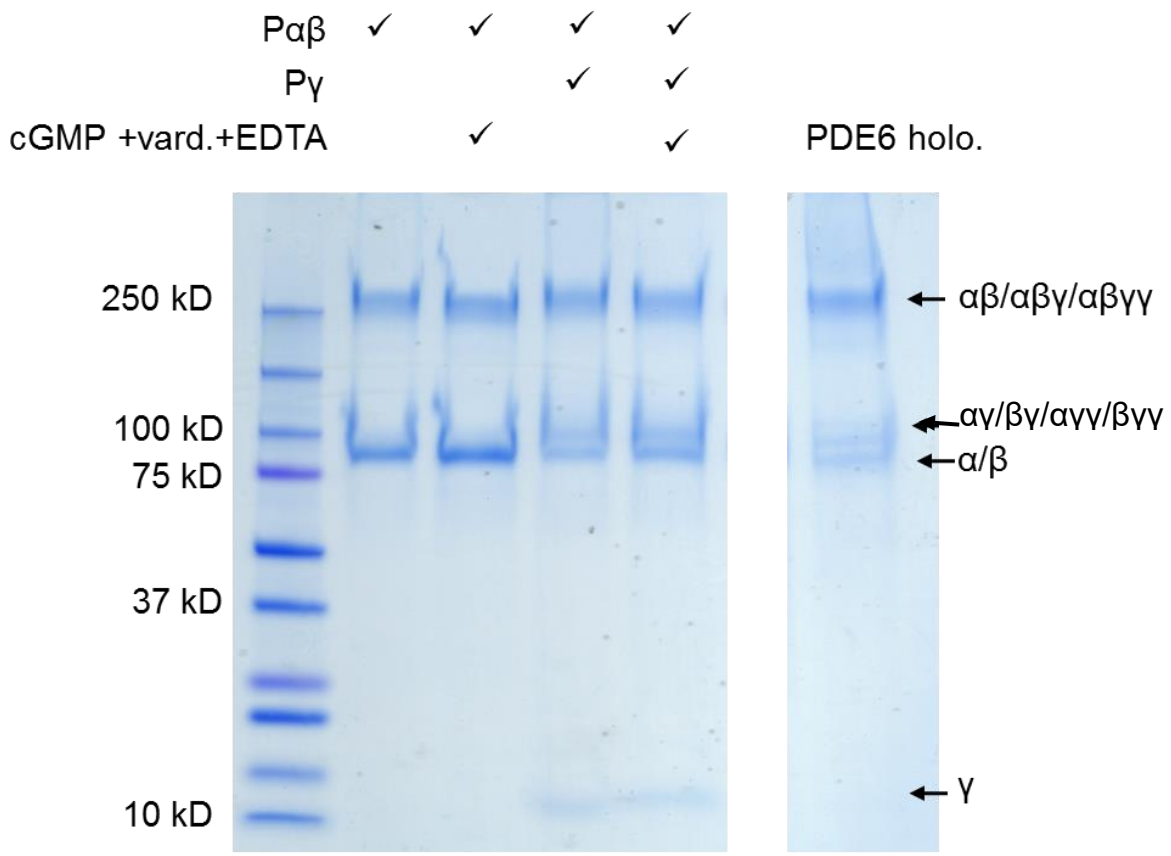

Fig. 1B Cross-linking reactions were separated on gradient SDS-PAGE, resulting in two or three distinct bands for each reaction condition.

purified PDE6, was also included as a control to compare with condition 4. From the resulting SDS-PAGE (Fig. 1B), distinct bands were visible at 250 and 90 kDa. For conditions 3, 4, and the holoenzyme, an additional band at 100 kDa was present, indicating either Pα or Pβ bound with Pγ.

Following LCMS/MS analysis, dead-end and cross-linked peptides were identified from each band, and the resulting calculated proportional intensities are presented in Table 1. When a cross-link was identified in more than one band within a lane, the average proportional intensity was reported. Standard deviation of each cross-linked peptide within a lane, for each lane, and was found to be consistently within 0.1 (10%), with two exceptions: β817- β763 in condition 1 (Pαb alone) and condition 2 (Pαβ with allosteric cGMP), which had a standard deviation of 0.1 and 0.2, respectively. Technical variation within each lane (biochemical condition) was calculated by calculating the pooled standard deviation of all replicate incidences, and was within 0.10. Given that the overall technical variation is about 0.10, any change in percent intensity greater than 0.20 can be considered significant in terms of relative cross-linking propensity when comparing one biochemical condition to another.

Dead-end cross-links were used to detect changes in residue reactivity and cross-linking propensity of cross-linked residues. Some cross-links were unchanged from one situation to another, such as β817-β826, which maintains a consistent percent intensity of ~0.8-1.1 (except for the reduction by half the percent intensity in the native holoenzyme), and β817- β827 which is consistently ~0.25-0.39. Most of the other cross-linked peptides undergo significant changes in percent intensity from one biochemical situation to another. Notably, β826-β827 maintains a constant percent intensity until both allosteric cGMP and Pγ are bound, which indicates a

Table 1

m/z	z	Peptide 1	Peptide 2	sub-unit	AA 1	AA 2	Mean Proportional Intensity: Pαβ only	Pαβ +cGMP	Pαβ +Pγ	recons. PDE6	holo PDE6
551.8281	4	VVDK(553.3588)FHIPQEALVR	LK(1787.9934)R	α	534	581	1.295	0.176	0.23	0.178	0.174
753.4062	4	SQNPLAK(1260.6424)LHGSSILER	K(1887.0214)DIFQDMVK	α	620	447	0.421	0.208	0.39	0.231	0.729
757.4059	4	SQNPLAK(1276.6373)LHGSSILER	K(1887.0214)DIFQDM(Ox)VK	α	620	447	0.313	---	0.45	---	---
588.9935	3	TMFQK(440.2747)IVDQSK	K(1461.7538)R	α	683	677	1.259	1.024	0.68	0.231	1.656
588.3008	4	ALADEYETK(1051.5550)MK	NK(1435.6905)ADELPK	α	819	765	0.062	---	---	---	---
799.402	3	ALADEYETK(1097.5605)MK	GLEEEK(1435.6905)QK	α	819	827	0.551	2.115	2.05	2.271	1.821
804.7332	3	ALADEYETK(1097.5605)M(Ox)K	GLEEEK(1451.6854)QK	α	819	827	0.275	0.418	---	1.257	0.831
503.7685	4	GLEEEK(1051.5550)QK	NK(1097.5605)ADELPK	α	827	765	0.431	0.91	---	0.494	---
665.4039	4	K(1301.7959)FQIPQEVLVR	ILK(1493.8606)EVLPGPAK	β	532	490	0.031	---	0.04	---	---
589.3216	3	TMFQK(440.2747)IVDESK	K(1462.7378)R	β	681	675	1.118	---	---	---	---
748.7424	3	ALADEYEAK(1007.5651)VK	NK(1373.7078)AAELPK	β	817	763	0.642	1.705	0.3	0.776	0.231
778.7407	3	ALADEYEAK(1097.5605)VK	ALEEDQK(1373.7078)K	β	817	826	0.949	1.066	0.85	1.009	0.466
513.5274	4	ALADEYEAK(814.4436)VK	K(1373.7078)ETTAK	β	817	827	0.258	0.392	0.22	0.246	0.14
513.5274	4	ALADEYEAK(814.4436)VK	ETTAK(1373.7078)K	β	817	832	0.213	0.165	0.17	0.22	0.197
716.8768	4	ALADEYEAKVK(814.4436)ALEEDQK	ETTAK(2187.0947)K	β	819	832	---	---	---	---	0.82
492.772	4	ALEEDQK(1007.5651)K	NK(1097.5605)AAELPK	β	826	763	---	0.16	---	---	0.036
592.3184	3	ALEEDQK(814.4436)K	K(1097.5605)ETTAK	β	826	827	0.168	0.182	0.16	0.081	0.086
592.3191	3	ALEEDQK(814.4436)K	ETTAK(1097.5605)K	β	826	832	---	0.137	0.11	---	0.085

Table 1. For each cross-linked peptide identified, the mean proportional intensity was calculated in each biochemical condition. In cases where only one of the cognate dead-end peptides was found, the value is underlined. Dashed indicated cases in which neither one was found. AA1 and AA2 are arbitrary designations for the two amino acids participating in the cross-link.

Figure 2

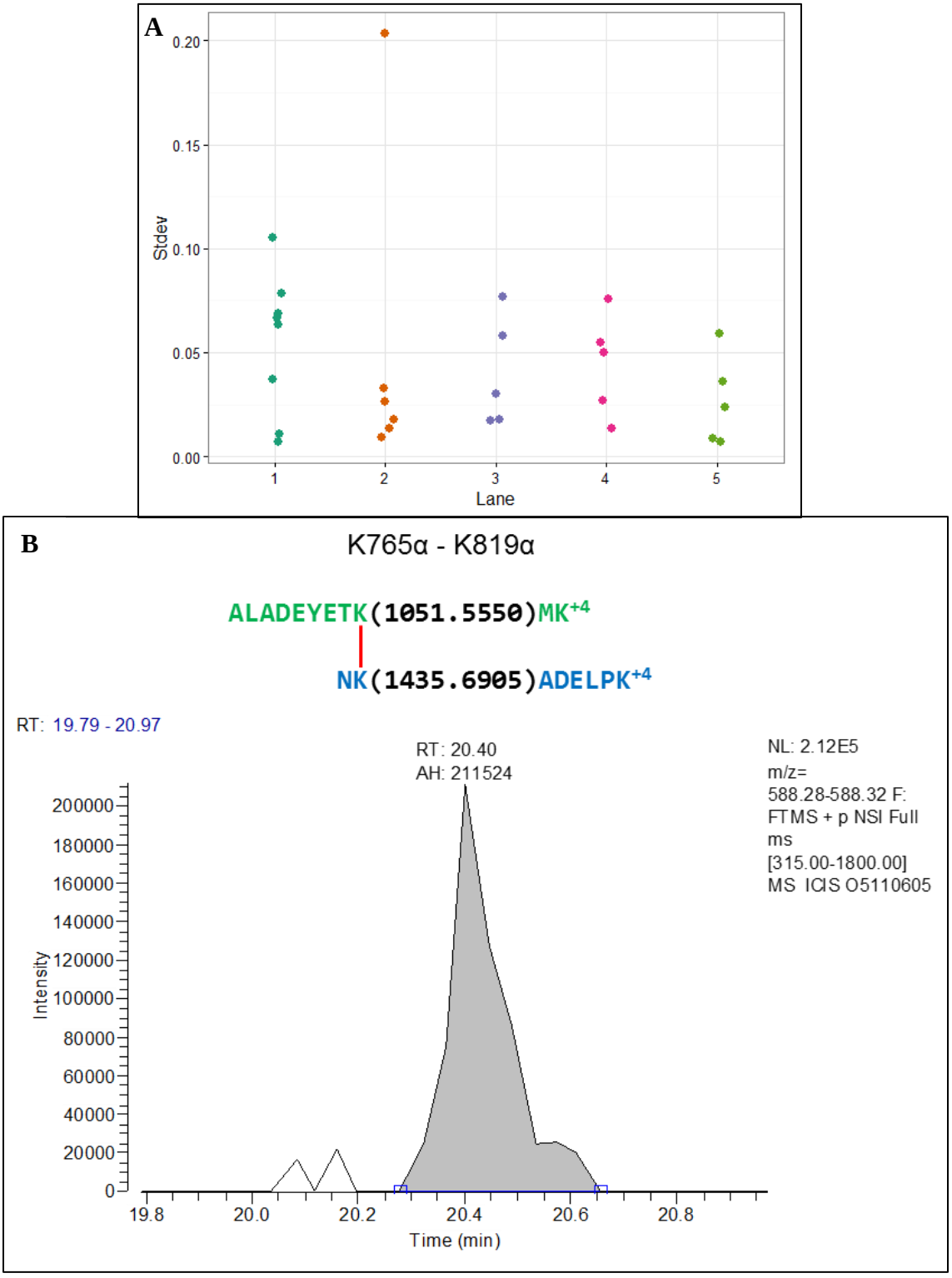

Fig. 2 A. Distribution of standard deviations for cross-linked peptides within each lane. Each lane corresponds to a different biochemical condition. **B.** A cross-linked peptide found only in the Pαβ condition, and its extracted ion chromatograph with peak height indicated.

Figure 3

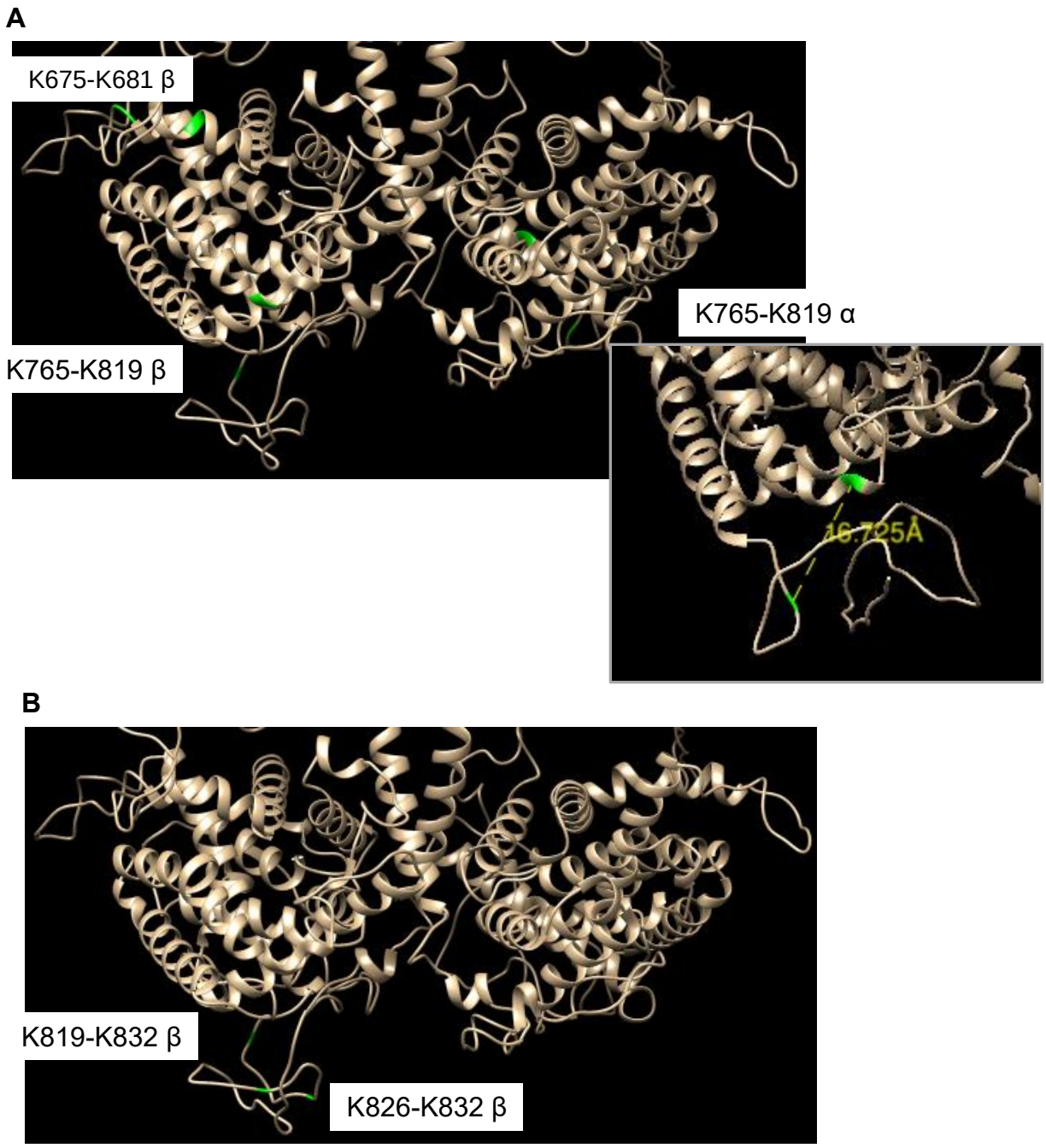

Fig 3. A. Catalytic domain of Pαβ (only), with three pairs of cross-linked lysines highlighted in green. The inset shows a reverse-side view. **B.** Catalytic domain of PDE6 (Pγ and cGMP not shown). A set of three cross-linked lysines is highlighted in green. Models shown are based on final_model.pdb [4].

potentially important region responding to the tandem effects of both regulatory ligands. These two residues are on an extended loop at the end of the catalytic domain, so this reduction in percent cross-linking propensity is consistent with previous experiments which showed Pγ directly blocking the active site of the catalytic domain [99, 104]. And since allosteric binding of cGMP enhances binding of Pγ, it is reasonable that we see this effect more distinctly in the holoenzyme condition.

3.4 Discussion

The identification of structural elements within the catalytic domain which reflect allosteric binding of ligands is congruent with previous work [41, 103, 100, 107]. However, none of the cross-links were in the H- or M- loops, which have previously been identified as exhibiting important structural features for Pγ binding [107]. This is not entirely surprising given the relatively interior situation of these loops and comparative lack of lysine residues. Surprisingly, condition four, which is the reconstituted holoenzyme, bears several differences to the natively purified holoenzyme. The natively purified holoenzyme yielded more cross-linked peptides than the reconstituted enzyme, and featured a cross-linked peptide for which the dead-end links were not found, meaning β819 and β827 were either cross-linked together or not at all, so they exhibit high propensity for cross-linking with each other. Further experimental replicates will be useful for confirming these results. Vardenafil and EDTA, which were both present in condition four but not in with the holoenzyme, or some alteration to Pαβ during trypsinization of Pγ, may account for these differences. Or, perhaps Pγ can exhibit multiple binding conformations such that is contacts different residues on the surface of Pαβ than would be found with PDE6 purified in native conformation.

Considering previous research which indicates a reciprocal enhancement of binding of the Pγ1-60 and Pγ63-87, it would be interesting to conduct additional experiments which return a sampling of crosslinks from the GAF domain in addition to the catalytic domain to determine the extent to which binding of Pγ and cGMP propagate through Pα and Pβ, and the structural basis for the inter-domain allosterism reported here and elsewhere. Many fundamental questions remain unanswered, including how the binding of Pγ subunits in GAF domains is structurally propagated to the distal catalytic domains, and the structural basis for the synergistic binding of cGMP and Pγ subunits to GAF domains.

Recent developments in nanodisc technology present intriguing possibilities for this work [106]. Pαβ mounted on a nanodisc could not only improve cross-linking efficiency, but also provide a more physiologically relevant context for the interactions within and between subunits. Transducin could be included in the cross-linking experiments to further characterize the "transducisome" [99]. While there is some evidence that membrane binding does not affect cGMP binding activity [100], such an experiment would provide confirmation that it also does not affect Pγ binding activity.

Chapter 4. Summary and Contribution of Thesis

Protein multifunctionality has recently been recognized as a widespread phenomenon that underlies the complex genotype/phenotype relationship [108]. Contextual information inside the cell, such as local pH and ligand concentration, presence of interaction partners and posttranslational modifications, modulate the component and conformation of proteins and protein complexes to regulate protein function outcome. Consistent with this idea, more and more proteins have been observed to exist in conformational equilibrium [84, 109] and a single amino acid substitution can completely change the fold and function of a protein [110]. Consequently, structural information specific to the cellular context is important to understand complex processes inside the cell. Recent progress in structural proteomics has laid important foundation work. However, measurements to elucidate conformational changes under specific biochemical conditions can reveal underlying mechanisms of complex cellular processes.

Over the past several years with the developments in bioinformatics, CXMS has gradually grown into a method of choice especially for challenging biological systems. CXMS provides a sensitive and robust approach to elucidate spatial proximity of amino acids and offers valuable structural insights. Besides generating binary results to elucidate spatial proximity of cross-linked residues, quantitative CXMS data can potentially shed light on conformational changes. The idea has indeed been employed by multiple studies to reveal large domain rearrangements in different biochemical states. Although biochemical conclusions from these studies, derived from drastic changes in MS signal intensity from several cross-linked pairs that cluster in 3-D space, are likely correct, multiple physicochemical factors can impact cross-linking yield.

In this thesis, we perceive that the quantity of surface modified peptides provides important contextual information about the cross-linked residues regarding the local environment, thus correlates with their reactivity towards the cross-linker. Furthermore, we hypothesize that we can deconvolute the impacts of residue solvent accessibility and pKa values by using surface modified peptides to potentially infer distance information from MS signal intensity of the cross-linked peptides. By considering quantitative MS data of surface modified peptides and separating residue reactivity and distance, we are able to provide additional information on the nature of conformational changes in distance biochemical states.

To test this idea, we used the structurally well-characterized *E. coli* Hsp90, HtpG, as a model system and obtained quantitative CXMS data from two distinct HtpG conformations. Contrary to conventional practice, we did not observe any obvious correlation between the MS signal intensity of cross-linked peptides and the distance of cross-linked residues. Our data demonstrate that both the pKa values and solvent accessibility of the cross-linked residues contribute to the reactivity of the cross-linked Lys residues. Furthermore, after reactivity normalization of cross-linked residues, an improved correlation could be observed between the MS signal intensity of cross-linked peptides and the distance of cross-linked residues. Normalization to the cognate surface modified peptides allows one to correct for the local environment of the amino acid side chains.

PDE6 represents an intriguing challenge for the study of protein complexes, and its unique role in vision lends it particular biomedical relevance. Previously, we have used structural information derived from chemical cross-linking and electron microscopy to build a computational model of PDE6 holoenzyme [41], which reveals a unique open configuration for PDE6 catalytic domains that is distinct from the crystal structure of *apo* PDE2 [111]. The distinct

open configuration provides structural insights on two unique features of PDE6 in PDE family enzymes, namely the inhibitory Pγ subunit and the diffusion-control catalysis rate.

To further understand the underlying mechanisms of allosteric regulators, the inhibitory Pγ subunit and the allosteric cGMP, we carried out quantitative CXMS analysis and compared four different allosteric states of PDE6 effector enzyme. After reactivity normalization, we observed a tight distribution of cross-linking propensity among cross-linked pairs within identical allosteric states, indicating minimal perturbation of protein conformation under our cross-linking conditions. In addition, we observed substantial conformational changes in catalytic domains, elicited by allosteric cGMP binding in distal GAF domains. Our data reveals structural elements that mediate allosteric regulation of PDE6 enzyme, providing biochemical insights on the coupling of cellular cGMP levels and PDE6 activation-deactivation cycle.

Considering the robustness of the CXMS approach, additional structural information may be gained by using other kinds of cross-linking reagents in an effort to sample areas other than the catalytic domain. Also, cross-linking of PDE6 *in situ*, after rod outer segment purification but prior to hypotonic extraction, may serve as an additional level of biochemical experimental control, since the membrane-bound enzyme should match the reconstituted version. The methods outlined in this work provide a platform upon which to understand cross-linked peptides within proteins and complexes. The value of this research to the study of vision, protein interactions, and the general operations of cells makes further research potentially quite profitable to society as a whole.

References

1. Holton, J. M. and Frankel, K. A. (2010) 'The minimum crystal size needed for a complete diffraction data set', *Acta Crystallographica Section D: Biological Crystallography*, 66(4), pp. 393–408.
2. Loquet, A., Gardiennet, C. and Böckmann, A. (2010) 'Protein 3D structure determination by high-resolution solid-state NMR', *Comptes Rendus Chimie. Academie des sciences*, 13(4), pp. 423–430.
3. Elmlund, D., Elmund, H. (2015) Cryogenic Electron Microscopy and Single-Particle Analysis. *Ann Rev Biochem*. 84, pp. 499-517.
4. Bai, X.C., McMullan, G., Scheres, S.H. (2015) How Cryo-EM is revolutionizing structural biology. *Trends Biochem Sci*. 40(1), pp. 49-57
5. Robinson, C. V, Sali, A. and Baumeister, W. (2007) 'The molecular sociology of the cell', *Nature*, 450(7172), pp. 973–982.
6. Hoelz, A., Glavy, J. S. and Beck, M. (2016) 'Toward the atomic structure of the nuclear pore complex: when top down meets bottom up'. *Nature Structural & Molecular Biology*. 23(7), pp. 624–630.
7. Bui, K. H., Von Appen, A., Diguilio, A. L., Ori, A., Sparks, L., Mackmull, M. T., Bock, T., Hagen, W., Andrés-Pons, A., Glavy, J. S. and Beck, M. (2013) 'Integrated structural analysis of the human nuclear pore complex scaffold'. *Cell*. 155(6), pp. 1233–1243.
8. Hernández, H., Dziembowski, A., Taverner, T., Séraphin, B. and Robinson, C. V (2006) 'Subunit architecture of multimeric complexes isolated directly from cells.', *EMBO reports*, 7(6), pp. 605–610.

9. Duan, Z., Andronescu, M., Schutz, K., McIlwain, S., Kim, Y. J., Lee, C., Shendure, J., Fields, S., Blau, C. A. and Noble, W. S. (2010) 'A three-dimensional model of the yeast genome.', *Nature*, 465(7296), pp. 363–367.

10. Kikhney, A. G. and Svergun, D. I. (2015) 'A practical guide to small angle X-ray scattering (SAXS) of flexible and intrinsically disordered proteins', *FEBS Letters. Federation of European Biochemical Societies*, 589(19), pp. 2570–2577.

11. Vinothkumar, K. R. (2015) 'Membrane protein structures without crystals, by single particle electron cryomicroscopy', *Current Opinion in Structural Biology*, 33, pp. 103–114.

12. Konermann, L., Pan, J. and Liu, Y.-H. (2011) 'Hydrogen exchange mass spectrometry for studying protein structure and dynamics.', *Chemical Society Reviews*, 40(3), pp. 1224–1234.

13. Micsonai, A., Wien, F., Kernya, L., Lee, Y.-H., Goto, Y., Réfrégiers, M. and Kardos, J. (2015) 'Accurate secondary structure prediction and fold recognition for circular dichroism spectroscopy.', *Proc Natl Acad Sci U S A*, 112(24), pp. E3095-103.

14. Hernández, H., Dziembowski, A., Taverner, T., Séraphin, B. and Robinson, C. V (2006) 'Subunit architecture of multimeric complexes isolated directly from cells.', *EMBO reports*, 7(6), pp. 605–610.

15. Wu, B., Peisley, A., Richards, C., Yao, H., Zeng, X., Lin, C., Chu, F., Walz, T. and Hur, S. (2013) 'Structural basis for dsRNA recognition, filament formation, and antiviral signal activation by MDA5.', *Cell*, 152(1–2), pp. 276–289.

16. Leitner, A., Faini, M., Stengel, F. and Aebersold, R. (2016) ‘Crosslinking and Mass Spectrometry: An Integrated Technology to Understand the Structure and Function of Molecular Machines’, *Trends in Biochemical Sciences*, 41(1), pp. 20-32.

17. Merkley, E. D., Rysavy, S., Kahraman, A., Hafen, R. P., Daggett, V. and Adkins, J. N. (2014) ‘Distance restraints from crosslinking mass spectrometry: mining a molecular dynamics simulation database to evaluate lysine-lysine distances.’, *Protein Science*, 23(6), pp. 747–759.

18. Rappsilber, J. (2011) ‘The beginning of a beautiful friendship: Cross-linking/mass spectrometry and modelling of proteins and multi-protein complexes’, *Journal of Structural Biology*, 173(3), pp. 530–540.

19. Fischer, L., Chen, Z. A. and Rappsilber, J. (2013) ‘Quantitative cross-linking/mass spectrometry using isotope-labelled cross-linkers.’, *Journal of proteomics*, 88, pp. 120–128.

20. Kluger, R. and Alagic, A. (2004) ‘Chemical cross-linking and protein-protein interactions-a review with illustrative protocols.’, *Bioorganic chemistry*, 32(6), pp. 451–472.

21. Barysz, H., Kim, J. H., Chen, Z. A., Hudson, D. F., Rappsilber, J., Gerloff, D. L. and Earnshaw, W. C. (2015) ‘Three-dimensional topology of the SMC2/SMC4 subcomplex from chicken condensin I revealed by cross-linking and molecular modelling.’, *Open biology*, 5:150005.

22. Stengel, F., Aebersold, R. and Robinson, C. V (2012) ‘Joining forces: integrating proteomics and cross-linking with the mass spectrometry of intact complexes.’, *Molecular & Cellular Proteomics*, 11(3), p. R111.014027-3.

23. Chu, F., Baker, P. R., Burlingame, A. L. and Chalkley, R. J. (2010) 'Finding chimeras: a bioinformatics strategy for identification of cross-linked peptides.', *Molecular & Cellular Proteomics*, 9(1), pp. 25–31.

24. Cooper, B. (2011) 'The Problem with Peptide Presumption and Low Mascot Scoring', *Proteome*, 10, pp. 1432–1435.

25. Trnka, M. J., Baker, P. R., Robinson, P. J. J., Burlingame, A L. and Chalkley, R. J. (2014) 'Matching cross-linked peptide spectra: only as good as the worse identification.', *Molecular & Cellular Proteomics*, 13(2), pp. 420–434.

26. Bandyopadhyay, P. and Kuntz, I. D. (2009) 'Computational investigation of kinetics of cross-linking reactions in proteins: importance in structure prediction.', *Biopolymers*, 91(1), pp. 68–77.

27. Mädler, S., Bich, C., Touboul, D. and Zenobi, R. (2009) 'Chemical cross-linking with NHS esters: A systematic study on amino acid reactivities', *Journal of Mass Spectrometry*, 44(5), pp. 694–706.

28. Schmidt, C., Zhou, M., Marriott, H., Morgner, N., Politis, A. and Robinson, C. V (2013) 'Comparative cross-linking and mass spectrometry of an intact F-type ATPase suggest a role for phosphorylation.', *Nature communications*, 4(May 2013), p. 1985.

29. Chen, Z. A., Jawhari, A., Fischer, L., Buchen, C., Tahir, S., Kamenski, T., Rasmussen, M., Lariviere, L., Bukowski-Wills, J.-C., Nilges, M., Cramer, P. and Rappsilber, J. (2010) 'Architecture of the RNA polymerase II-TFIIF complex revealed by cross-linking and mass spectrometry.', *The EMBO journal*, 29(4), pp. 717–726.

30. Guo, X., Bandyopadhyay, P., Schilling, B., Young, M. M., Fujii, N., Aynechi, T., Guy, R. K., Kuntz, I. D. and Gibson, B. W. (2008) 'Partial acetylation of lysine residues improves intraprotein cross-linking.', *Analytical chemistry*, 80(4), pp. 951–960.

31. Alipanahi B., Krislock N., Ghodsi A., Wolkowicz H., Donaldson L., Li M. (2013) 'Determining Protein Structures from NOESY Distance Constraints by Semidefinite Programming.' *Journal of Computational Biology*, 20(4), pp. 296-310.

32. Rappsilber, J. (2011) 'The beginning of a beautiful friendship: Cross-linking/mass spectrometry and modelling of proteins and multi-protein complexes', *Journal of Structural Biology*, 173(3), pp. 530–540.

33. Walzthoeni, T., Leitner, A., Stengel, F. and Aebersold, R. (2013) 'Mass spectrometry supported determination of protein complex structure', *Current Opinion in Structural Biology*, 23(2), pp. 252–260.

34. Merkley ED, Cort JR, & Adkins JN (2013) 'Cross-linking and mass spectrometry methodologies to facilitate structural biology: finding a path through the maze.' *J Struct Funct Genomics* 14(3), pp. 77-90.

35. Tran, B. Q., Goodlett, D. R. and Goo, Y. A. (2016) 'Advances in protein complex analysis by chemical cross-linking coupled with mass spectrometry (CXMS) and bioinformatics', *Biochimica et Biophysica Acta (BBA) - Proteins and Proteomics*, 1864(1), pp. 123–129.

36. Sinz, A., Arlt, C., Chorev, D. and Sharon, M. (2015) 'Chemical cross-linking and native mass spectrometry: A fruitful combination for structural biology', *Protein Science*, 24(8), pp. 1193–1209.

37. Young, M. M., Tang, N., Hempel, J. C., Oshiro, C. M., Taylor, E. W., Kuntz, I. D., Gibson, B. W. and Dollinger, G. (2000) 'High throughput protein fold identification by using

experimental constraints derived from intramolecular cross-links and mass spectrometry.', *Proc Natl Acad Sci U S A*, 97(11), pp. 5802–5806.

38. Chu, F., Shan, S., Moustakas, D. T., Alber, F., Egea, P. F., Stroud, R. M., Walter, P. and Burlingame, A. L. (2004) 'Unraveling the interface of signal recognition particle and its receptor by using chemical cross-linking and tandem mass spectrometry', *Proc Natl Acad Sci U S A*, 101(47), pp. 16454–16459.

39. Chu, F., Maynard, J. C., Chiosis, G., Nicchitta, C. V and Burlingame, A. L. (2006) 'Identification of novel quaternary domain interactions in the Hsp90 chaperone, GRP94.', *Protein science*, 15(6), pp. 1260–1269.

40. Wu, B., Peisley, A., Richards, C., Yao, H., Zeng, X., Lin, C., Chu, F., Walz, T. and Hur, S. (2013) 'Structural basis for dsRNA recognition, filament formation, and antiviral signal activation by MDA5.', *Cell*, 152(1–2), pp. 276–289.

41. Zeng-elmore, X., Gao, X., Pellarin, R., Schneidman-duhovny, D., Zhang, X., Kozacka, K. A, Tang, Y., Sali, A., Chalkley, R. J., Cote, R. H. and Chu, F. (2014) 'Molecular Architecture of Photoreceptor Phosphodiesterase Elucidated by Chemical Cross-Linking and Integrative Modeling', *Journal of Molecular Biology*, 426(22), pp. 3713–3728.

42. Schneidman-Duhovny, D., Rossi, A., Avila-Sakar, A., Kim, S. J., Velázquez-Muriel, J., Strop, P., Liang, H., Krukenberg, K. A., Liao, M., Kim, H. M., Sobhanifar, S., Dötsch, V., Rajpal, A., Pons, J., Agard, D. A., Cheng, Y. and Sali, A. (2012) 'A method for integrative structure determination of protein-protein complexes', *Bioinformatics*, 28(24), pp. 3282–3289.

43. Rinner, O., Seebacher, J. and Walzthoeni, T. (2008) 'Identification of cross-linked peptides from large sequence databases', *Nature Methods*, 5(4), pp. 315–318.

44. Lee, Y. J. (2009) ‘Probability-Based Shotgun Cross-Linking Sites Analysis’, *Journal of the American Society for Mass Spectrometry*, 20(10), pp. 1896–1899.

45. Panchaud A, Singh P, Shaffer SA, & Goodlett DR (2010) 'xComb: a cross-linked peptide database approach to protein-protein interaction analysis.' *Journal of Proteome Research* 9(5), pp: 2508-2515.

46. Du, X., Chowdhury, S., Manes, N., Wu, S., Mayer, M. U., Adkins, J., Anderson, G., and Smith, R. (2011) 'Xlink-identifier: an automated data analysis platform for confident identifications of chemically cross-linked peptides using tandem mass spectrometry.' *Journal of Proteome Research* 10(3), pp. 923-931.

47. Xu H, Hsu PH, Zhang L, Tsai MD, and Freitas MA (2010) 'Database search algorithm for identification of intact cross-links in proteins and peptides using tandem mass spectrometry.' *Journal of Proteome Research* 9(7), pp. 3384-3393.

48. Hoopmann, M., Zelter, A., Johnson, R., Riffle, M., MacCoss, M., Davis, T., and Moritz, R. (2015) 'Kojak: efficient analysis of chemically cross-linked protein complexes.' *Journal of Proteome Research*, 14(5), pp. 2190-2198.

49. Lasker K, Förster F, Bohn S, Walzthoeni T, Villa E, Unverdorben P, Beck F, Aebersold R, Sali A, Baumeister W. (2012). 'Molecular architecture of the 26S proteasome holocomplex determined by an integrative approach'. *Proc Natl Acad Sci U S A*, 109(5), pp. 1380-1387.

50. Sanowar, S., Singh, P., Pfuetzner, R. A., André, I., Zheng, H., Spreter, T., Stryndaka, C., Gonen, T., Baker, D., Goodlett, D., Miller, S. (2010). 'Interactions of the Transmembrane Polymeric Rings of the Salmonella enterica Serovar Typhimurium Type III Secretion System.' *mBio*, 1(3), e00158–10.

51. Robinson PJ, Bushnell DA, Trnka MJ, Burlingame AL, & Kornberg RD (2012) 'Structure of the mediator head module bound to the carboxy-terminal domain of RNA polymerase II.' *Proc Natl Acad Sci U S A* 109(44), pp. 17931-17935.

52. Liu, H., Zhang, H., Weisz, D. A., Vidavsky, I., Gross, M. L. and Pakrasi, H. B. (2014) 'MS-based cross-linking analysis reveals the location of the PsbQ protein in cyanobacterial photosystem II', *Proc Natl Acad Sci U S A*, 111(12), pp. 4638–4643.

53. Shi, Y., Pellarin, R., Fridy, P. C., Fernandez-Martinez, J., Thompson, M. K., Li, Y., Wang, Q. J., Sali, A., Rout, M. P. and Chait, B. T. (2015) 'A strategy for dissecting the architectures of native macromolecular assemblies.', *Nature methods*, 12(12), pp. 1135–1138.

54. Liu, F., Rijkers, D. T. S., Post, H. and Heck, A. J. R. (2015) 'Proteome-wide profiling of protein assemblies by cross-linking mass spectrometry', *Nature methods*, 12(12), pp. 1179-1184

55. Walzthoeni, T., Joachimiak, L. A., Rosenberger, G., Röst, H. L., Malmström, L., Leitner, A., Frydman, J. and Aebersold, R. (2015) 'xTract: software for characterizing conformational changes of protein complexes by quantitative cross-linking mass spectrometry.', *Nature methods*, 12(12), pp. 1185–1190.

56. Street, T. O., Zeng, X., Pellarin, R., Bonomi, M., Sali, A., Kelly, M. J. S., Chu, F. and Agard, D. a (2014) 'Elucidating the mechanism of substrate recognition by the bacterial hsp90 molecular chaperone.', *Journal of molecular biology*, 426(12), pp. 2393–2404.

57. Guo, X., Bandyopadhyay, P., Schilling, B., Young, M. M., Fujii, N., Aynechi, T., Guy, R. K., Kuntz, I. D. and Gibson, B. W. (2008) 'Partial acetylation of lysine residues improves intraprotein cross-linking.', *Analytical chemistry*, 80(4), pp. 951–960.

58. Bandyopadhyay, P. and Kuntz, I. D. (2009) ‘Computational investigation of kinetics of cross-linking reactions in proteins: importance in structure prediction.’, *Biopolymers*, 91(1), pp. 68–77.

59. Toews J, Rogalski JC, Clark TJ, & Kast J (2008) 'Mass spectrometric identification of formaldehyde-induced peptide modifications under in vivo protein cross-linking conditions.' *Anal. Chim. Acta*, 618(2), pp. 168-183.

60. Liu F & Goshe MB (2010) 'Combinatorial electrostatic collision-induced dissociative chemical cross-linking reagents for probing protein surface topology.' *Anal. Chem.* 82(14), pp. 6215-6223.

61. Toews J, Rogalski JC, & Kast J (2010) 'Accessibility governs the relative reactivity of basic residues in formaldehyde-induced protein modifications.' *Anal Chim Acta* 676(1-2), pp. 60-67.

62. Taipale M, Jarosz DF, & Lindquist S (2010) 'HSP90 at the hub of protein homeostasis: emerging mechanistic insights.' *Nat Rev Mol Cell Biol* 11(7), pp. 515-528.

63. Trepel J, Mollapour M, Giaccone G, & Neckers L (2010) 'Targeting the dynamic HSP90 complex in cancer.' *Nat Rev Cancer* 10(8), pp. 537-549.

64. Krukenberg KA, Street TO, Lavery LA, & Agard DA (2011) 'Conformational dynamics of the molecular chaperone Hsp90.' *Quarterly Rev Biophys* 44(2), pp. 229-255.

65. Jakob U, Lilie H, Meyer I, & Buchner J (1995) 'Transient interaction of Hsp90 with early unfolding intermediates of citrate synthase. Implications for heat shock in vivo.' *J Biol Chem* 270(13), pp. 7288-7294.

66. Wiech H, Buchner J, Zimmermann R, & Jakob U (1992) 'Hsp90 chaperones protein folding in vitro.' *Nature* 358(6382), pp. 169-170.

67. Zhao, R., Davey, M., Hsu, Y. C., Kaplanek, P., Tong, A., Parsons, A. B., Krogan, N., Cagney, G., Mai, D., Greenblatt, J., Boone, C., Emili, A. and Houry, W. A. (2005) 'Navigating the chaperone network: An integrative map of physical and genetic interactions mediated by the hsp90 chaperone', *Cell*, 120(5), pp. 715–727.

68. McClellan, A. J., Xia, Y., Deutschbauer, A. M., Davis, R. W., Gerstein, M. and Frydman, J. (2007) 'Diverse cellular functions of the Hsp90 molecular chaperone uncovered using systems approaches.', *Cell*, 131(1), pp. 121–135.

69. Taipale, M., Tucker, G., Peng, J., Krykbaeva, I., Lin, Z. Y., Larsen, B., Choi, H., Berger, B., Gingras, A. C. and Lindquist, S. (2014) 'A quantitative chaperone interaction network reveals the architecture of cellular protein homeostasis pathways', *Cell*, 158(2), pp. 434–448.

70. Obermann WM, Sondermann H, Russo AA, Pavletich NP, & Hartl FU (1998) 'In vivo function of Hsp90 is dependent on ATP binding and ATP hydrolysis.' *J Cell Biol* 143(4), pp. 901-910.

71. Panaretou, B., Prodromou, C., Roe, S. M., O'Brien, R., Ladbury, J. E., Piper, P. W., & Pearl, L. H. (1998). 'ATP binding and hydrolysis are essential to the function of the Hsp90 molecular chaperone in vivo.' *The EMBO Journal*, 17(16), pp. 4829–4836.

72. Grenert JP, Johnson BD, & Toft DO (1999) 'The importance of ATP binding and hydrolysis by hsp90 in formation and function of protein heterocomplexes.' *J Biol Chem* 274(25), pp. 17525-17533.

73. Street TO, Lavery LA, & Agard DA (2011) 'Substrate binding drives large-scale conformational changes in the Hsp90 molecular chaperone.' *Molecular Cell* 42(1), pp. 96-105.

74. Street, T. O., Lavery, L. A., Verba, K. A., Lee, C. T., Mayer, M. P. and Agard, D. A. (2012) ‘Cross-monomer substrate contacts reposition the Hsp90 N-terminal domain and prime the chaperone activity.’ *Journal of Molecular Biology*, 415(1), pp. 3–15.

75. Genest, O., Reidy, M., Street, T. O., Hoskins, J. R., Camberg, J. L., Agard, D. a, Masison, D. C. and Wickner, S. (2013) ‘Uncovering a region of heat shock protein 90 important for client binding in E. coli and chaperone function in yeast.’ *Molecular cell*, 49(3), pp. 464–473.

76. Lorenz, O. R., Freiburger, L., Rutz, D. A., Krause, M., Zierer, B. K., Alvira, S., Cuéllar, J., Valpuesta, J. M., Madl, T., Sattler, M. and Buchner, J. (2014) ‘Modulation of the Hsp90 chaperone cycle by a stringent client protein.’ *Molecular cell*, 53(6), pp. 941–953.

77. Park SJ, Kostic M, & Dyson HJ (2011) 'Dynamic interaction of Hsp90 with its client crotein p53.' *J Mol Biol* 411(1), pp. 158-173.

78. Krukenberg KA, Forster F, Rice LM, Sali A, & Agard DA (2008) 'Multiple conformations of E. coli Hsp90 in solution: insights into the conformational dynamics of Hsp90.' *Structure* 16(5), pp. 755-765.

79. Krukenberg KA, Southworth DR, Street TO, & Agard DA (2009) 'pH-dependent conformational changes in bacterial Hsp90 reveal a Grp94-like conformation at pH 6 that is highly active in suppression of citrate synthase aggregation.' *J Mol Biol* 390(2), pp. 278-291.

80. Southworth DR & Agard DA (2008) 'Species-dependent ensembles of conserved conformational states define the Hsp90 chaperone ATPase cycle.' *Mol Cell* 32(5), pp. 631-640.

81. Kahraman, A., Herzog, F., Leitner, A., Rosenberger, G., Aebersold, R. and Malmström, L. (2013) ‘Cross-Link Guided Molecular Modeling with ROSETTA.' *PLoS ONE*, 8(9)

82. Merkley, E. D., Rysavy, S., Kahraman, A., Hafen, R. P., Daggett, V. and Adkins, J. N. (2014) ‘Distance restraints from crosslinking mass spectrometry: mining a molecular dynamics simulation database to evaluate lysine-lysine distances.’ *Protein science*, 23(6), pp. 747–759.

83. Alexandrescu AT, Abeygunawardana C, & Shortle D (1994) 'Structure and dynamics of a denatured 131-residue fragment of staphylococcal nuclease: a heteronuclear NMR study'. *Biochemistry* 33(5), pp. 1063-1072.

84. James LC, Roversi P, & Tawfik DS (2003) 'Antibody multispecificity mediated by conformational diversity.' *Science* 299(5611), pp. 1362-1367.

85. Celikel, R., McClintock, R. A., Roberts, J. R., Mendolicchio, G. L., Ware, J., Varughese, K. I. and Ruggeri, Z. M. (2003) ‘Modulation of alpha-thrombin function by distinct interactions with platelet glycoprotein Ib alpha.' *Science*, 301(5630), pp. 218–221.

86. Jeffery CJ (2004) 'Molecular mechanisms for multitasking: recent crystal structures of moonlighting proteins.' *Curr Opin Struct Biol* 14(6), pp. 663-668.

87. Alexander PA, He Y, Chen Y, Orban J, & Bryan PN (2009) 'A minimal sequence code for switching protein structure and function.' *Proc Natl Acad Sci U S A* 106(50), pp. 21149-21154.

88. Park B & Levitt M (1996) 'Energy functions that discriminate X-ray and near native folds from well-constructed decoys.' *J Mol Biol* 258(2), pp. 367-392.

89. Park BH, Huang ES, & Levitt M (1997) 'Factors affecting the ability of energy functions to discriminate correct from incorrect folds.' *J Mol Biol* 266(4), pp. 831-846.

90. Wei L, Huang ES, & Altman RB (1999) 'Are predicted structures good enough to preserve functional sites?' *Structure* 7(6), pp. 643-650.

91. Young JC, Schneider C, & Hartl FU (1997) 'In vitro evidence that hsp90 contains two independent chaperone sites.' *FEBS Lett* 418(1-2), pp. 139-143.

92. Scheibel T, Weikl T, & Buchner J (1998) 'Two chaperone sites in Hsp90 differing in substrate specificity and ATP dependence.' *Proc Natl Acad Sci U S A* 95(4), pp. 1495-1499.

93. Dixit A & Verkhivker GM (2012) 'Probing molecular mechanisms of the Hsp90 chaperone: biophysical modeling identifies key regulators of functional dynamics.' *PLoS One* 7(5), pp. e37605.

94. Retzlaff, M., Hagn, F., Mitschke, L., Hessling, M., Gugel, F., Kessler, H., Richter, K. and Buchner, J. (2010) 'Asymmetric Activation of the Hsp90 Dimer by Its Cochaperone Aha1.' *Molecular Cell*, 37(3), pp. 344–354.

95. Pettersen EF, Goddard TD, Huang CC, Couch GS, Greenblatt DM, Meng EC, Ferrin TE. (2004) 'UCSF Chimera--a visualization system for exploratory research and analysis.' *J Comput Chem* 25(13), pp. 1605-1612

96. Olsson, M, Sondergaard, C, Rostkowski M, and Jensen J. (2011) 'PROPKA3: consistent treatment of internal and surface residues in empirical pKa predictions.' *Journal of Chemical Theory and Computation* 7(2), pp. 525-537.

97. Matte, S. L., Laue, T. M., & Cote, R. H. (2012). 'Characterization of conformational changes and protein-protein interactions of rod photoreceptor phosphodiesterase (PDE6).' *Journal of Biological Chemistry*, 287(24), pp. 20111–20121

98. Goc, A., Chami, M., Lodowski, D. T., Bosshart, P., Moiseenkova-Bell, V., Baehr, W., Engel, A., Palczewski, K. (2010). 'Structural characterization of the rod cGMP phosphodiesterase 6.' *Journal of Molecular Biology*, 401(3), pp. 363–373

99. Guo, L. W., Hajipour, A. R. and Ruoho, A. E. (2010) 'Complementary interactions of the rod PDE6 inhibitory subunit with the catalytic subunits and transducin', *Journal of Biological Chemistry*, 285(20), pp. 15209–15219.

100. Yamazaki, A., Hayashi, F., Matsuura, I. and Bondarenko, V. A. (2011) 'Binding of cGMP to the transducin-activated cGMP phosphodiesterase, PDE6, initiates a large conformational change involved in its deactivation', *FEBS Journal*, 278(11), pp. 1854–1872.

101. Zhang, X. J., Gao, X. Z., Yao, W., Cote, R. H. (2012). 'Functional mapping of interacting regions of the photoreceptor phosphodiesterase (PDE6) γ-subunit with PDE6 catalytic dimer, transducin, and regulator of G-protein signaling9-1 (RGS9-1).' *Journal of Biological Chemistry*, 287(31), pp. 26312–26320

102. Muradov, H., Boyd, K. K. & Artemyev, N. O. (2004) 'Structural determinants of the PDE6 GAFa domain for binding the inhibitory gamma-subunit and noncatalytic cGMP.' *Vision Res.* 44, pp. 2437–2444.

103. Zhang, X. J., Cahill, K. B., Elfenbein, A., Arshavsky, V. Y. & Cote, R. H. (2008) 'Direct allosteric regulation between the GAF domain and catalytic domain of photoreceptor phosphodiesterase PDE6.' *J. Biol. Chem.* 283, pp. 29699–29705.

104. Granovsky, A. E., Natochin, M. and Artemyev, N. O. (1997) 'The Gamma Subunit of Rod cGMP- Phosphodiesterase Blocks the Enzyme Catalytic Site', *Biochemistry*, 272(18), pp. 11686–11689.

105. Pentia DC, Hosier S, Collupy RA, Valeriani BA, Cote RH. (2005) ‘Purification of PDE6 isozymes from mammalian retina.’ *Methods Mol Biol*; 307, pp. 125–140.

106. Denisov, I., Sligar, S. (2016) ‘Nanodiscs for structural and functional studies of membrane proteins.’ *Nature Structural & Molecular Biology*, 23(6), pp. 481–486

107. Barren, B., Gakhar, L., Muradov, H., Boyd, K. K., Ramaswamy, S. and Artemyev, N. O. (2009) ‘Structural basis of phosphodiesterase 6 inhibition by the C-terminal region of the gamma-subunit’, *The EMBO journal*, 28(22), pp. 3613–3622.

108. Chapple, C. E., Robisson, B., Spinelli, L., Guien, C., Becker, E. and Brun, C. (2015) ‘Extreme multifunctional proteins identified from a human protein interaction network.’ *Nature communications*, 6 (May), pp. 7412.

109. Celikel, R., McClintock, R. A., Roberts, J. R., Mendolicchio, G. L., Ware, J., Varughese, K. I. and Ruggeri, Z. M. (2003) ‘Modulation of alpha-thrombin function by distinct interactions with platelet glycoprotein Ibalpha’, *Science*, 301(5630), pp. 218–221.

110. Alexander PA, He Y, Chen Y, Orban J, & Bryan PN (2009) 'A minimal sequence code for switching protein structure and function.' *Proc Natl Acad Sci U S A* 106(50), pp. 21149-21154.

111. Pandit, J., Forman, M. D., Fennell, K. F., Dillman, K. S. and Menniti, F. S. (2009) ‘Mechanism for the allosteric regulation of phosphodiesterase 2A deduced from the X-ray structure of a near full-length construct.’ *Proc Natl Acad Sci U S A*, 106(43), pp. 18225–18230.